

A Kinetic Model Describing the Processivity of Myosin-V

Karl I. Skau^{*‡}

Rebecca B. Hoyle^{*}

^{*} Department of Mathematics and Statistics,
University of Surrey, Guildford, Surrey, GU2 7XH, UK

Matthew S. Turner[‡]

[‡] Department of Physics,
Warwick University, Coventry, CV4 7AL, UK

Abstract

The precise details of how myosin-V coordinates the biochemical reactions and mechanical motions of its two head elements to engineer effective processive molecular motion along actin filaments remain unresolved. We compare a quantitative kinetic model of the myosin-V walk, consisting of five basic states augmented by two further states to allow for futile hydrolysis and detachments, with experimental results for run lengths, velocities, and dwell times and their dependence on bulk nucleotide concentrations and external loads in both directions. The model reveals how myosin-V can use the internal strain in the molecule to synchronise the motion of the head elements. Estimates for the rate constants in the reaction cycle and the internal strain energy are obtained by a computational comparison scheme involving an extensive exploration of the large parameter space. This scheme exploits the fact that we have obtained analytic results for our reaction network, e.g. for the velocity but also the run length, diffusion constant and fraction of backward steps. The agreement with experiment is often reasonable but some open problems are highlighted, in particular the inability of such a general model to reproduce the reported dependence of run length on ADP. The novel way that our approach explores parameter space means that any confirmed discrepancies should give new insights into the reaction network model.

Key words: Myosin, motor, processivity, mechanism, model, optimisation.

Introduction

A myosin protein is an ATPase which gains enzymatic activity by attaching to an actin filament (1, 2, 3). The myosin proteins use the chemical energy released in ATP-hydrolysis to create directed mechanical motion. More than 100 proteins have been identified as belonging to the myosin superfamily and they are organised into some 18 subgroups (1, 4). A myosin is identified by a conserved 80 kDa motor domain and it is usually assumed that all the myosin motor proteins share the same biochemical reaction pathway when hydrolysing ATP (1). The most studied of the myosins is the non-processive (muscle) myosin II whose main reaction path is found to follow the classical Lymn–Taylor scheme (5) describing the correlation of mechanical and chemical events.

Myosin-V is a dimeric protein involved in the intracellular transport of a variety of cargos. The neck region of the two head elements is three times the length of the corresponding region of the myosin II heads (6). It is generally assumed that the long neck region acts as a lever arm and the size of the protein makes it possible for myosin-V to walk hand-over-hand (7, 8, 9, 10) following the helical repeat of actin. Myosin-V was the first molecular motor shown to be *processive* along actin filaments (11). Previously established processive motors like kinesin and dynein use microtubules as the track for their processive directed motion, or in the case of RNA polymerase, DNA. Naturally, there has been much interest both in confirming the processive motion of myosin-V and in gaining insight into the details of the molecule's motion using recent developments in experimental techniques (7, 8, 9, 10, 11, 12, 13, 14, 15, 16, 17, 18, 19, 20, 21, 22, 23, 24, 25, 26). Similarly, several theoretical models of the myosin-V walk with different levels of detail have been proposed (12, 13, 20, 22, 23, 24, 25, 27, 28, 29, 30, 31).

How myosin-V coordinates the biochemical reactions and mechanical motions of the two head elements of the protein to become an effective processive molecular motor is an open question. While there is a general agreement on the enzymatic reaction path for a *single* myosin head, the details of how myosin-V keeps the two heads' reaction cycles in phase is still unresolved. Likewise, there is still a lack of understanding of how external forces directly influence the kinetic mechanism of the walk and what role the internal strain in the molecule plays. As a result of the large number of measurements made on myosin-V in the last years, this is an appropriate time to make more detailed, quantitative models of the myosin-V walk, and to see how such models compare with what is found experimentally.

The outline of the article is as follows: we first establish our model for

the processive walk of myosin-V and explain the model’s underlying assumptions. In the results section we present analytic results for our, rather general, reaction network. These include the velocity, run length, diffusion constant and fraction of backward steps. These observable quantities are functions that depend on a number of parameters (mainly characteristic energies for the various transitions between states). The unknown parameters are estimated by optimising the agreement of the model with a chosen representative set of experimental results. This approach, which is based on defining a cost-function, is outlined in the third section. We then present quantitative results for the optimised parameters and compare them with available experimental data and end with a discussion. Agreement with experiment is generally reasonable, though we are unable to explain the trend of the run length with varying ADP concentration. We discuss how our approach might be used to explore such possible discrepancies between existing reaction network models and experiment, generating new insights into the myosin V stepping mechanism.

Model

The reaction network for our model is sketched in Fig. 1. The main reaction cycle contains states 1 to 5. In state 4 the rear head starts its reaction cycle by releasing ADP, while the front head will not react before the whole cycle has been completed making it the new rear head. In state 5 the rear head is in the rigor state with no nucleotide attached, and the rear head will detach rapidly from the actin filament when it reacts with ATP from the bulk. The mechanical motion that moves the rear head into the front position is found experimentally to happen in two steps (22, 25), from position 1 to position 2, and then from position 2 to position 3. In state 3 the front head is weakly attached to actin, so only one head is strongly attached in states 1 to 3, making these the more vulnerable states for total detachment of the molecule from actin. When inorganic phosphate P_i is released from the lead head, going from state 3 to state 4, the myosin binds strongly to actin and the lead head makes the so-called “powerstroke”. Since the rear head is still attached, the lead head will not achieve the usual post-powerstroke angle with the actin filament, which will cause internal strain in the molecule. This is consistent with electron microscopy (EM) images (9, 20) which show strongly bound myosin-V to take a position similar to a telemark-skier’s stance, indicating large internal strain in the molecule.

The model given above for the main walk follows fairly closely the inter-

mediate states proposed by Rief et al. (12) which accounts for the most important experimental findings for myosin-V (13). Note that there is still disagreement in the literature as to which states are present in the main reaction cycle for the processive motion of myosin-V (see for instance Refs. (13, 22, 23, 24, 28, 30)). A natural consequence of the microscopic size of the motor protein is that both mechanical and chemical effects are important. We expect the external force, due for instance to the viscous drag of a cargo vesicle, to most strongly influence the mechanical steps in the cycle which involve translational motion.

The main reaction path is reversible in the sense that one could, in principle, run the ATP hydrolysis reaction in reverse by pulling the motor backwards with an external force. (This would not be a very effective way to produce ATP since the motor is kinetically tuned to move efficiently in one direction only). It is important for a model which aims to investigate the mechanism of a motor protein to also include the effect of futile cycles and detachment rates. Futile cycles consume ATP without creating any net movement of the molecule while detachment limits the run length of the molecule. If, in an evolutionary sense, myosin-V were to tune the reaction rates of the motor domain it might well seek to maximise the forward velocity (requiring “weak binding”). However, it should probably also seek to minimise the impact of futile cycles and detachment rates (requiring “strong binding”). The kinetic parameters that arise might then be expected to correspond to a suitable compromise solution. We remark that the computational scheme for exploring parameter space that we will later describe could be used in the future to explore such evolutionary pressures and trends.

There will in general be a large number of possible unfavourable pathways, but we will assume that among these there is one dominant futile reaction cycle which takes place when the ADP in state 4 of the main cycle (Fig. 1) detaches from the front head before the rear head moving to state 6. In the futile cycle the front head then reacts with a new ATP molecule so that the molecule returns back to state 2 without having created any net movement. Similarly, we will identify what we believe to be the dominant detachment rate. We make the conjecture that the molecule is most vulnerable to detachment when only one head is attached to actin, as in state 2 (due to the high internal strain in the molecule, state 1 is a short lived unstable state). We will assume that detachment from state 2 dominates over all other detachment rates. The mechanism of detachment will be the release of ADP followed by the binding of ATP to the rear head so that myosin-V detaches completely from the actin filament before strong

attachment is achieved by the front head (state 7, Fig. 1).

The assumption we have made so far is that the main cycle is described well by the qualitative model of Rief et al. (12) where in addition the mechanical motion of the rear head to the front is taken in two steps. Furthermore, we assume that there is one futile cycle that dominates over all others, and that this futile cycle involves states 2 and 4 in the main cycle. Lastly, we assume that the detachment rate at state 2 dominates all others. The complete model we have outlined (shown in Figs. 1 and 2) is a minimal realistic model for the walk of a molecular motor like myosin-V.

Reaction rates

The reaction rates between the different states are described by Arrhenius expressions:

$$w_i = \tau^{-1} e^{-(G_i^\ddagger + \Delta G_i)/k_B T}, \quad (1)$$

where τ is the fundamental time scale of the reaction and k_B is the Boltzmann constant. (We use the notation where u_i and w_i are the forward and backward rates, respectively, away from state i (32)). G_i^\ddagger is the energy barrier between state i and its neighbour state in the forward direction, while ΔG_i is the energy difference between the two states. We set $T = 298$ K in this article. The total energy balance for the ATP hydrolysis is

$$\Delta G_{\text{hyd}} = k_B T \ln \left(\frac{[\text{ATP}]}{[\text{ADP}][\text{P}_i]} \right) + \sum_{i=2}^5 \Delta G_i, \quad (2)$$

where the nucleotide concentrations are made dimensionless by dividing by the concentrations at the reference states for ΔG_i , $[\text{ATP}]^0 = [\text{ADP}]^0 = [\text{P}_i]^0 = 1$ M. The standard free energy $\Delta G^{(0)} = \sum \Delta G_i \simeq 32.5$ [kJ/mol] (33) which is close to $13 k_B T$, while $\Delta G_{\text{hyd}} \simeq 25 k_B T$ at cellular conditions (2).

For the main cycle, one ends up with a total of ten reaction rates. The first four rate constants in the main cycle are related to the mechanical movement (see Figs. 1 and 3);

$$u_1 = \tau_d^{-1}, \quad (3)$$

$$w_2 = \tau_d^{-1} e^{-(E_{\text{strain}} - f_{\text{ex}} (d_W - \frac{1}{2} f_{\text{ex}}/k_H))/k_B T}, \quad (4)$$

$$u_2 = \tau_d^{-1} e^{-(G_2^\ddagger + f_{\text{ex}} (d_D + \frac{1}{2} f_{\text{ex}}/k_H) + bE_{\text{strain}})/k_B T}, \quad (5)$$

$$w_3 = \tau_d^{-1} e^{-(G_2^\ddagger + \Delta G_2)/k_B T}, \quad (6)$$

where τ_d is a hydrodynamic time-scale related to diffusion over one step-length and f_{ex} is the component of the external force parallel to the actin

filament. The mechanical step is separated into a so-called working stroke of $d_W \simeq 25$ nm and a diffusional sub-step of $d_D \simeq 11$ nm (see Fig. 3), as indicated by experimental findings (22, 25), giving a total step size $d = d_W + d_D \simeq 36$ nm (11, 12, 18). Thus we neglect the (weak) external force dependence of the diffusional step size in u_1 but capture the dominant effect of the force in, e.g. retarding the activated rate u_2 and in distorting the metastable shape of the bound arm in state 2 (through the $\sim f_{\text{ex}}^2$ terms in the exponents of w_2 and u_2). The total internal strain in the molecule E_{strain} defines an effective Hookeian spring constant, k_{H} , related to the compliance in the motor and neck region of the myosin head:

$$E_{\text{strain}} = \frac{1}{2} k_{\text{H}} d_W^2, \quad (7)$$

where we have assumed that the molecule is fully strained in state 1.

State 2 is in mechanical equilibrium. The position of the hinge/neck in state 2 is influenced by the magnitude of the external force, which gives rise to the energy term $1/2 f_{\text{ex}}^2/k_{\text{H}}$ in w_2 and u_2 (Eqs. (4) and (5)). When moving from state 2, either back to state 1 or forward to state 3, the molecule increases its internal strain by E_{strain} or $bE_{\text{strain}} = 1/2 k_{\text{H}} d_D^2$ respectively (Fig. 3). Using the latter expression together with Eq. (7) gives $b = (d_D/d_W)^2 \simeq 0.2$. Since $E_{\text{strain}} > bE_{\text{strain}}$ there is a bias in the forward direction away from state 2, making the molecule a Brownian ratchet (34).

Notice that the external force f_{ex} is defined to be positive in the direction opposite to the movement of the myosin-V molecule, and that only the influence of the force parallel to the actin filament is taken into account. (The external force is of course a vector quantity, with a possible important influence on the walk arising from the normal component of the force (35, 36).) The external force will accelerate or slow down the two reaction rates w_2 and u_2 away from state 2, depending on the sign of f_{ex} .

Experimentally, it is found that there is one rate-limiting step in the walk of myosin-V (14, 15, 16). At large external force, f_{ex} , one or more sub-steps that couple to the force, will become rate-limiting. A phenomenological way to model this is (11)

$$\tau_* = \tau_1 + \tau_2 e^{f_{\text{ex}} d_{\text{eff}}/k_{\text{B}}T}. \quad (8)$$

Here τ_* is the (average) dwell time for one step, while τ_1 and τ_2 are the dwell times of the force independent and dependent sub-steps respectively, and the external force couples to a distance d_{eff} . When fitting experimental data to this phenomenological equation, naively one would expect $d_{\text{eff}} \simeq 36$ nm

which is the average step length. Instead it was found that d_{eff} is between 10–15 nm. From our model this scale emerges quite naturally, since the external force couples to the diffusional search governed by rate u_2 which gives $\tau_* \simeq \tau_1 + 1/u_2$. From Eq. (5) we have

$$u_2 = A e^{-f_{\text{ex}}(d_D + \frac{1}{2} f_{\text{ex}}/k_H)/k_B T}, \quad (9)$$

where A is some constant. Here d_D is 11 nm while the correction term $\frac{1}{2} f_{\text{ex}}/k_H$ of the position of the hinge in state 2 is of the order of 8 nm when close to stall force. It is satisfying that this is consistent with the value of d_{eff} cited above and indicates that the way we include the two substeps in our model is reasonable. (See Ref. (27) for a discussion of the limitations of Eq. (8)).

The reaction rates for states with both heads attached to actin (see Fig. 1) are given by

$$u_3 = \tau^{-1} e^{-G_3^\ddagger/k_B T}, \quad (10)$$

$$w_4 = [\text{P}_i] \tau^{-1} e^{-(G_3^\ddagger + \Delta G_3 - (1-b)E_{\text{strain}})/k_B T}, \quad (11)$$

$$u_4 = \tau^{-1} e^{-G_4^\ddagger/k_B T}, \quad (12)$$

$$w_5 = [\text{ADP}] \tau^{-1} e^{-(G_4^\ddagger + \Delta G_4)/k_B T}, \quad (13)$$

$$u_5 = [\text{ATP}] \tau^{-1} e^{-G_5^\ddagger/k_B T}, \quad (14)$$

$$w_1 = \tau^{-1} e^{-(G_5^\ddagger + \Delta G_5)/k_B T}, \quad (15)$$

where the nucleotide concentrations and $[\text{P}_i]$ in Eqs. (11)–(14) are given as dimensionless quantities (see comments under Eq. (2)). τ is a microscopic time scale related to the characteristic oscillation frequency of the protein. The free parameters in the model are the activation energies G_i^\ddagger , the energy differences ΔG_i , and the strain energies. When an estimate is made for these free parameters, the resulting energy landscape (Fig. 4) gives directly all the predicted reaction rates, and the model's predictions for myosin-V's velocity and run lengths along the actin filament (see Appendix A). Note that τ is *not* really an independent variable since it can be absorbed into the activation energies; $1/\tau \exp(G_i^\ddagger) \equiv 1/\tau_0 \exp(G_i^\ddagger + \ln(\tau_0/\tau))$.

As a measurement of the deviation away from equilibrium one can introduce the parameter

$$\Gamma = \prod_{j=1}^5 \frac{u_j}{w_j} = e^{\Delta G_{\text{hyd}}/k_B T} e^{-f_{\text{ex}}d/k_B T}, \quad (16)$$

which gives the thermodynamic driving force for the molecular motor (32, 37). To fulfill detailed balance we have $\Gamma = 1$ at equilibrium (37). As expected from the energy balance the external force appears in Γ as $f_{\text{ex}}d$; this is the total work done by the motor when completing one reaction cycle with step-length d . From Eq. (16) it is clear how the external force shifts the apparent equilibrium constant of the hydrolysis reaction. This coupling between the external force and the free energy of the hydrolysis of ATP, gives directly the thermodynamic upper bound on the stall-force $f_{\text{stall}} = \Delta G_{\text{hyd}}/d$ ($\simeq 2.8$ pN at cellular conditions). (The presence of futile cycles will influence the upper bound on the stall-force, but this correction is found to be insignificant for our (best) model).

The reaction rates for the futile cycle are given by

$$u_{4,6} = u_4 e^{-\alpha E_{\text{strain}}/k_{\text{B}}T}, \quad (17)$$

$$w_{6,4} = w_5 e^{-\alpha E_{\text{strain}}/k_{\text{B}}T}, \quad (18)$$

$$u_{6,2} = u_5, \quad (19)$$

$$w_{2,6} = w_1 e^{-E_{\text{strain}}/k_{\text{B}}T} e^{-f_{\text{ex}}(d_D + \frac{1}{2} f_{\text{ex}}/k_{\text{H}})/k_{\text{B}}T}. \quad (20)$$

Here $u_{i,j}$ and $w_{i,j}$ are the reaction rates from state i to state j . Using the fact that the two head elements are structurally identical, we make the assumption that the front head has to have the neck at a similar angle to that between the rear neck and the actin filament in step 4 of the main cycle to make it possible for ADP to be released or bind to the myosin motor domain (Eqs. (17) and (18)). To achieve this, the front head has to overcome the strain energy in the molecule in state 4 which creates an energy barrier αE_{strain} for the ADP release reaction governed by rate $u_{4,6}$ (see Fig. 3). In this way myosin-V synchronises the biochemical reactions of the two heads.

To move from state 2 to state 6 (Fig. 1), the molecule has to increase the internal strain by E_{strain} without the energy from the hydrolysis reaction, (Eq. (20)), so there is a very low probability for the futile cycle to run in reverse (effectively becoming a useful reaction path way). The reaction rates in the futile cycle follow the reaction rates for the main cycle except for the extra barrier caused by the strain in the molecule, so there is only one new parameter that appears in the the model. In principle αE_{strain} could be estimated if the elastic moduli of the different parts of the molecule were known, by making a detailed structural model based on EM measurements (20) and crystal structures (38, 39) of myosin-V (see also Vilfan (30)). We will not attempt to do this here, but leave αE_{strain} as an undetermined en-

ergy barrier, an energy barrier used by myosin-V to synchronise the reaction cycles of the two head elements.

The detachment from state 2 takes place if the ADP detaches from the rear head before the front head becomes weakly bound. The relevant reaction rates are

$$u_{2,7} = u_4, \quad (21)$$

$$w_{7,2} = w_5, \quad (22)$$

$$u_7 = u_5 e^{|f_{\text{ex}}|\delta/k_{\text{B}}T}. \quad (23)$$

The external force will increase the detachment rate of the single head (an effect we neglect when both heads are strongly attached, which should be a good approximation when considering the strain level in the molecule). Pulling experiments on S1 give an apparent interaction distance of $\delta = 2.4$ nm (21) for the external force (Eq. (23)).

An extended model where we would also consider the reattachment rate of motors is of course possible (40) but not particularly relevant since the local bulk concentration of motors and of actin target sites is usually not well-controlled in an experiment. Our main focus in this model will be single-molecule experiments and their predictions.

In our model we use the fact that the two head regions of the myosin-V protein are identical and have identical biochemical reaction paths. It might seem at first that this would be an obstacle to the processive motion of the protein, since the reactions of the two heads must be out of phase to ensure that at all times at least one of the two heads is strongly attached to the actin filament. However, evidence has been found in EM experiments that the intra-molecular strain affects the two bound heads asymmetrically (9, 20). The model outlined above shows explicitly how this asymmetrical strain can be used by the two heads to coordinate their reaction cycles and to minimise the impact of the futile cycles and detachment rates.

Parameters

The fundamental time scales, τ and τ_{d} can be estimated using the Stokes–Einstein relation. τ_{d} is related to the diffusion time of the whole head element (with a “diameter” of $\simeq 30$ nm) over the step size $d_{\text{W}} \simeq 25$ nm, which gives $\tau_{\text{d}} \simeq 10^{-5}$ s. Similarly, τ is related to movement of a few nanometres, where the relevant length scale is the thickness of the head element, giving $\tau \simeq 10^{-8}$ s. Note that any difference between τ or τ_{d} in the different steps will be absorbed into the activation energies G_i^{\ddagger} (see comment

under Eq. 15) so we are only interested in the order of magnitude of these time scales. Similarly, the activation energies will also be modified by the bulk pH and ionic strength, even though the influence of these solution properties are not included explicitly into the model.

Estimates of some of the activation energies are available through chemical kinetic reaction rate measurements, but we will not try to guess the values of the activation energies but leave them all as free parameters. The model of the myosin-V walk outlined above is a fairly detailed model containing seven different states and 13 reaction rates, still the number of undetermined parameters is relatively low. We have the four activation energies, G_i^\ddagger , three independent energy differences ΔG_i (where one energy difference will be dependent because of Eq. (2)), and finally two terms connected to the strain level in the molecule, E_{strain} and αE_{strain} . We are therefore left with nine undetermined parameters in our model of the myosin-V walk, which is a small number considering that the model is able to predict not only the walk's dependence on the bulk concentrations of ATP, ADP, and P_i , but also how the external force couples to the walk. The model is also detailed in its prediction of how the internal strain influences the walk and the level of strain in the molecule. Our model is therefore over-determined with respect to the available experimental data and provides many measurable predictions.

Optimisation

To search the parameter space computationally we define a *cost function* which quantifies the agreement between the model and the data. There is clearly some subjectivity involved in choosing the terms in the cost function: for example, one might be more inclined to include data that have been confirmed by several different research groups. We cannot investigate all possible permutations of our cost function since the optimisation approach is quite computationally demanding. However, the 17 experimental features that we identify, and encode in the cost function, are those that we expect a good model for the walk of myosin-V to reproduce. These include trends observed under variation of nucleotide bulk concentrations and the external force. Each term in the cost function was included to search for such a trend or to restrict the value of the energy jumps ΔG_i between substeps. Likewise, we specify variances to indicate how large a deviation from each target value we deem acceptable. The cost function, Δ , given in Appendix B, is constructed as a simple sum of 17 terms and each term gives an $O(1)$

contribution when within the accepted experimental error (as defined by our chosen variance). We believe that our cost function is a minimal encoding of the most important experimental trends, but it is possible to extend or modify our approach by including further or different data points if desired.

We do not choose arbitrarily what values the nine undetermined parameters should take but instead search the parameter space for favourable combinations using a technique based on simulated annealing (41) of the cost function. To make the search effective, we first evaluate the cost function at 50 million points in a parameter space of nine times $25 k_B T$. (This is the energy available in the hydrolysis reaction, Eq. (2), under cellular conditions. The internal energy E_{strain} and energy differences ΔG_i cannot be larger than the energy in the hydrolysis reaction, while there are no such limits in principle on the kinetic parameters and αE_{strain}). To make sure these points are evenly spread in the parameter space we use the Sobol quasi-random sequence (41, 42). The fifty points with the lowest cost function from the Sobol sampling were then passed to a simulated annealing routine, where the cost function is the “energy” term. The number of steps in the simulated annealing is chosen so that it is equal to the number of steps in a random walk over the average distance between the Sobol points.

An attractive feature of estimating the free parameters in the model like this is that it has some similarities to the way the molecular motor has tuned the same parameters through evolution to achieve physiologically required velocities and run lengths under variable cellular conditions.

Results

After optimising the parameters for our model (Table 1), it was found that there is one rate-limiting step, $u_4 = 14.7 s^{-1}$, corresponding to the largest value of G_i^\ddagger for $i = 2, \dots, 5$, which is the release of ADP from the rear head in state 4, Fig. 1. The ADP release rate is in quantitative agreement with kinetic measurements (11, 13, 14, 15, 16, 22, 24) which estimates u_4 between $10 s^{-1}$ to $20 s^{-1}$. From the model (Fig. 1) it can be seen why ADP release is the crucial reaction step for the myosin-V walk, since both the futile cycle and detachment depend on it. By slowing down the ADP release, myosin-V achieves a larger duty ratio for the myosin head, but more importantly, also reduces the flux around the futile cycle and similarly the detachment rate. Since the rate limiting step also determines the average velocity of the motor, there is a trade off when tuning the rate of u_4 . It is satisfying that the optimisation scheme of our model is able to reproduce the kinetic

tuning found experimentally. It is worth noting that no optimal solutions were found in other parts of the parameter space, i.e., no other possible combination of reaction rates could be found with either a different rate-limiting step or more than one rate-limiting step.

The optimised “best fit” model parameters, as given in Table 1, give rise to $u_5 = 0.3 \mu\text{M s}^{-1}$ for the attachment rate of ATP to the rear head in state 5, a prediction that is somewhat slower than experimental estimates of u_5 in the range from 0.6–1.5 $\mu\text{M s}^{-1}$ (22). The release of P_i is found to be fast when the front head is attached weakly to actin (state 3, Fig. 1) with $u_3 = 3200 \text{ s}^{-1}$, an order of magnitude above the lower bound from kinetic measurements $u_3 > 250 \text{ s}^{-1}$ (14).

It is a somewhat subtle point that the velocities and run lengths that our model predicts (see Appendix A) are independent of one aspect of that model, specifically whether the mechanical motion between state 3 and state 4 is assumed to happen before or during the release of P_i . This is in spite of the fact that the forms of Eqs. (10) and (11) *are* sensitive to this difference: the $(1 - b)E_{\text{strain}}$ term would appear in the exponential in u_3 and not in w_4 if the mechanical transition occurred before the phosphate release rather than during the phosphate release, as we assume here. The reason for this is that the optimization process fixes only the observable rates (u_3 and w_4). This appears to suggest that there may be some ambiguity in the value of the energy G_3^\ddagger that appears in these rates, depending on whether the motion between state 3 and state 4 happens before or during the release of P_i , i.e. whether the peak in the energy landscape occurs closer to state 4 or state 3 respectively. We can nonetheless determine the form of the equations by considering the kinetic measurements for P_i release. These are carried out using single myosin heads *without* internal strain. If, for the intact two-headed molecule, the $(1 - b)E_{\text{strain}}$ term was instead placed in the exponential in u_3 (and the peak in the energy landscape was close to state 4) then the rate for a *strain-free* transition, such as would be expected to be the case for single headed molecules, would be larger by a factor of $\exp[(1 - b)E_{\text{strain}}]$, giving rise to unrealistic phosphate release rates that would be four orders of magnitude higher than 3200 s^{-1} . This provides quantitative evidence that the power stroke of the front lever arm takes place *after* P_i is released, as is illustrated in Fig. 4 where the energy barrier between state 3 and state 4 is close to state 3.

We estimate the internal strain, $E_{\text{strain}} = 12.8 k_{\text{B}}T$ which gives a rigidity $\kappa = 120 k_{\text{B}}T \text{ nm} = 500 \text{ pN nm}^2$ for the lever arm (43), in agreement with other estimates in the literature (44). This gives a Young modulus of $Y = 0.6 \text{ [GPa]}$ assuming the myosin neck has an effective radius of 1 nm, which

is comparable to what is found in similar proteins (2). The strain barrier, αE_{strain} , preventing the futile cycle was found in the optimisation scheme to be $5.4 k_{\text{B}}T$, which slows down the release of ADP from the front head (state 4, Fig. 1) ~ 50 – 200 times compared to the rear head under changing nucleotide concentrations in the bulk. This is consistent with measurements reported by Rosenfeld and Sweeney (24).

Among the more important properties of myosin-V are its velocity and processivity along the actin filament. We are interested in how these two properties are influenced by the bulk concentrations of nucleotides and the presence of an external force in our model. In single molecule experiments, all of these parameters can be controlled and monitored, giving rise to direct measurements of their influence on the myosin-V walk.

The velocity of myosin-V has been measured at between 200 – 500 nm/s (13), which is consistent with the magnitude of the velocities predicted by the model. The velocity appears to follow a Michaelis–Menten like form in which it becomes independent of ATP at high ATP concentration, while linearly dependent on ATP at low ATP concentrations (Fig. 5). There is similarly found to be a strong dependence of the velocity on the ADP concentration. P_i only has a measurable influence on the velocity (and the run length) at very large excess concentrations, similarly to what is found experimentally (13, 23). When comparing the velocity dependence on concentration of ATP and ADP directly with experimental measurements (23), we find reasonable quantitative agreement (Fig. 5).

Our model reproduces the trend of velocity with increasing external force (see Fig. 6) found experimentally in Ref. (25). Note that our model only considers the external force parallel to the motion of myosin-V along actin, while in an experiment optical loads are usually applied both along the axis of movement and perpendicular to it (35, 36). This might explain some of the discrepancies observed at large external forces. When applying a negative external force (pulling in the forward direction), the velocity is not found to increase significantly as has also been found by (26). When the pulling force in the direction of the motion exceeds 2 pN, we find that the average velocity decreases, since the molecule tends, increasingly, to be pulled off the actin track thereby populating state 7 in the reaction cycle (Fig. 1) and reducing the forward motion. This reduction in the average velocity at large negative force was not observed by Clemen et al. (26).

Related to the velocity of myosin-V is the dwell time, t_d , defined by Eq. (49) in Appendix A, which is the average time it takes before the molecule takes a *forward* step (11, 27). Comparing the prediction of the model for the dependence dwell time on force with experimental results

(11, 25) reveals fair agreement for high ADP and high ATP concentration and the correct trend, though poor quantitative agreement, for high ATP but low ADP concentration (Fig. 7). However, the model is not able to reproduce the finding (11, 25) that the dwell time becomes independent of force at low ATP concentration.

An important parameter for a processive motor is the duty ratio (2), r_d , the average proportion of the time the head is strongly attached to actin. The duty ratio of myosin-V is found to be close to 90 % (24), while our model predicts even higher duty ratio at low forces (Fig. 8). As expected, the duty ratio is reduced at higher external force, since the mechanical motion from state 1 to state 3 is slowed down, and becomes rate-limiting around 1.6 pN at saturating ATP concentrations, which is consistent with experimental results of 1.5 pN (11, 13).

Baker et al. (23) have measured run lengths of myosin-V as a function of ADP and ATP concentrations. When looking at the dependence of the run length on the ATP concentration, our model predicts a decrease in run length when increasing the ATP concentration (Fig. 9), which is consistent with experimental results (23). The run length is found from our model by finding the eigenvalue of the matrix of rate constants which gives the slowest relaxation time in the system (see Appendix A). Since there is one dominating eigenvalue, we get a single exponential decay in run length.

We find a nonmonotonic dependency of the run length on the ADP concentration, as is also found experimentally. (The nonmonotonicity leads to the crossing over of the $[ADP] = 1$ mM and $[ADP] = 1$ μ M lines on Fig. 9 at low ATP concentrations.) However, while Baker et al. (23) finds a strong increase in the run length when decreasing the ADP concentration below $[ADP] = 1$ mM, our model predicts a decrease in the run length (Fig. 9). It is not immediately obvious why our model does not reproduce this experimental finding. It is clear that the model neglects many possible futile cycles and detachment rates and maybe even other possible useful reaction cycles. For instance in Baker et al. (23) it is suggested that myosin-V needs two useful reaction cycles to be able to function under variable conditions. Even though our model only has one main reaction cycle it seems to be able to reproduce many of the experimental findings under very different conditions, casting some doubt on this earlier assertion. It does not seem at all obvious that it would be of physiological advantage for myosin-V to reduce its run length under increase of the ADP concentration. This may suggest that futile cycles not included in our model play a role. Finally, this puzzle indicates that the ADP dependence of the run length is worthy of further experimental investigation.

The run length drops exponentially when increasing the force as shown in Fig. 10. The run length is also found to be very influenced by pulling in the *forward* direction (negative force). This can be understood by considering Fig. 8. The duty ratio increases with a negative external force since the mechanical movement from state 1 to state 3 is accelerated. This also makes it less likely that the molecule will end up in state 7 and detach (Fig. 1). At high negative external forces though, the run length is decreased, since the larger force is pulling the molecule off the actin track, Eq. (23). This non-monotonic behaviour in the run length as a function of force was not observed in a recent study (26) which found the run length of myosin-V to be fairly insensitive to both positive and negative external force over a large range of values. Note that our model probably exaggerates the increase in attachment rate of the front head to actin when pulled strongly in the forward direction. For a strong force the position of state 2 (Fig. 3) might change so much that the front head no longer is in the target zone slowing down the diffusion to the target site. If a correction for this had been included in our model we believe that the run length increase for a negative external force would be reduced.

Using Eq. 48, Fig. 11 shows the fraction of backwards steps is found to be low until around 2 pN, consistent with experimental findings (12, 26). As is shown in Fig. 11, the model predicts that the fraction of backwards steps are larger at low ATP concentrations, again in agreement with experimental results (11, 13).

A quantitative measure of the stochastic deviations from uniform constant-speed motion (Fig.12) is given by the so-called randomness ratio (27, 45), $\rho = 2D/Vd$, where D is the dispersion given by Eq. 50. The reciprocal of ρ gives a measure of the number of rate limiting steps, and for different ATP concentrations and external forces, it is found that the model gives only one rate limiting step. This is somewhat different than earlier theoretical predictions (27), and experimental measurements of the randomness ratio can be used to differentiate between theoretical models. At high forces ρ diverges because of the vanishing velocity close to stall force.

A biochemical reaction network is expected to be robust to small changes in the kinetic parameters (46). This robustness is needed to tackle both the natural changes that occur inside a cell during its lifetime and the fact that cellular biochemical reaction networks are highly interconnected, so a perturbation in one affects many others. A simple and effective robustness test is to see how the motion of the motors is affected by changes of $\pm 5\%$ in the different parameters. This also gives information on which parameters have the largest influence on for instance the velocity and run length of

the molecule in the model. Fig. 13 shows that G_4^\ddagger and to a lesser degree E_{strain} have the largest influence on the run length, while ΔG_4 is the only parameter which gives significant changes in the velocity when perturbed. The importance of G_4^\ddagger and ΔG_4 in controlling velocity and run length is to be expected, since these are the parameters determining the rate constants u_4 and w_4 for ADP release from and recapture by the rear head between states 4 and 5, which we have found to be the rate-limiting step.

Since the temperature enters explicitly in our equations, via the thermal energy scale $k_B T$, it is natural to look at how the temperature influences the run length and the velocity. Some caution should be noted though, since it is found that some of the free energy terms themselves are known to be directly dependent on temperature (24). Fig. 14 is obtained under the assumption that none of the energy terms depend strongly on temperature.

Discussion

Many reasonable and well justified models of the myosin-V's walk exist in the literature, but the majority of the models are of a qualitative nature and often introduce unnecessary (and uncontrolled) approximations when employed to obtain quantitative predictions. Of quantitative models in the spirit of this work, one interesting early study for myosin-V is due to Kolomeisky and Fisher (27) who considered a two state model which took some account of step-size variations. It was found that there is a substep in the walk of myosin-V creating another possible reaction pathway, as also suggested in some experiments (25, 47). One shortcoming in our model, is that the model does not allow for the possibility that the geometry or mechanics of the walk can change in different regimes, for instance at very different bulk concentrations or external forces. It is still an open question whether motor proteins change behaviour in a dramatic way in different regimes, but some evidence suggests that stepping length is influenced by force (22, 25, 26). Some recent papers (30, 31) have tried to explicitly calculate the different strain energies for the different step lengths, which would be helpful to clarify the detailed mechanism of the motion of myosin-V. One problem in such calculations is that several angles and rigidities are not well known so that the number of free parameters becomes very large.

There is necessarily some arbitrariness as to how many and which distinct states are included in a model, since the concept is strictly only a useful *approximation* to the complex, fluctuating motion of the protein. Several sub-states (and thereby sub-steps in the main reaction cycle) which have

been identified experimentally or on thermodynamic grounds (16, 39, 48) are not included in this model. This means that the sub-reaction rates between some of the states have been combined into one effective rate. Where possible we have chosen not to excessively “coarse-grain” the state-space, e.g. by classifying many states together into fewer, more broadly defined states. Philosophically this seems wise if one is not certain *a priori* that such coarse graining of state space won’t reduce the models precision or predictive power. We also feel that it is of value that the model takes into account all the steps where the protein reacts with smaller bulk molecules, since bulk concentration is something that can be controlled experimentally. Similarly, we wanted to separate out the different steps that are expected to couple to the external force. As a result, the proposed model can make direct predictions as to how the external force produced by an optical tweezer, for instance, should change the behaviour of the myosin-V walk. It is anyway important to remember that the complexity of a model such as ours is not really a function of the number of states but rather the number of parameters, which remains small, the interpretation of the parameters, which remains physically clear, and the reaction network topology.

The elastic strain in the molecule plays several roles in our model; most importantly, the strain in the molecule synchronises the chemical reactions of the two myosin heads. This is vital for making myosin-V an effective processive motor (22). The synchronisation is caused by the slowing down of the ADP release from the lead head compared to the rear head in state 4, since the internal strain makes it less likely for the lead head to have the optimal angle relative to the actin filament necessary for ADP release. A related benefit of this is that the slowing down of ADP release from the lead head minimises the impact of the futile cycle. Also, the strain biases the detached head to stay in the “target zone” (state 2, Figs. 1 and 2) when doing the (11 nm) biased diffusional search for the next attachment site on the actin filament. This bias both increases the velocity of the motor, since less time is used in the diffusional search for the next target site on the actin, and increases the processivity by decreasing the time spent with only one head strongly attached to the actin.

The model does not contain any direct dissipation of free energy ΔG_{diss} . Such dissipation by friction and heat loss caused by the non-equilibrium motion of the protein would reduce the total useful work that the molecular motor could do by reducing the effective free energy of the hydrolysis reaction $\Delta G_{\text{eff}} = \Delta G_{\text{hyd}} - \Delta G_{\text{diss}}$. We have not tried to quantify the size of ΔG_{diss} but assumed that it is relatively small. It would of course be possible to include ΔG_{diss} as an undetermined parameter even though we have

chosen not to do this here. The model does take into account the energy dissipated by the futile hydrolysis of ATP by the futile cycle (Fig. 1) which does no work and creates no net movement, but since αE_{strain} is estimated to be relative large, the release rate of ADP from the front head in state 4 (Fig. 1) is reduced two orders of magnitude compared to the release of the rear head. This indicates that myosin-V is a tightly coupled motor under all conditions and the futile cycle will not dissipate significant energy.

The starting point for our model was the qualitative model proposed by Rief *et al.* (12) and the observation that myosin-V has a so-called powerstroke movement and a diffusional search. There are several alternative mechanisms suggested in the literature, although they typically have a lot in common since there is general agreement on the single head reaction mechanism. One influential alternative model has been proposed by De La Cruz *et al.* (49) where the strong attachment of the front head to actin is triggered by the release of the rear head. It is also possible to envision there being several *parallel* reaction paths followed by the motor, where all these paths contribute significantly to the forward motion. It would be natural to assume that different paths dominate in different regimes, which would then provide a strategy for the motor to function well under varying conditions. One interesting example (23) of such a parallel reaction path mechanism, involved combining the Rief *et al.* and the De La Cruz *et al.* models into a version with two-paths. Taking into account the number of proposed models in the literature and then the possibility of different combinations of the various models, the number of permutations of possible models is clearly very large. We argue that a more quantitative analysis of the competing models would often be useful, e.g. using a computational scheme similar to that presented here.

We have presented a moderately detailed model of the walk of myosin-V, and compared the accuracy of the model with experimental measurements for velocities, run lengths, and dwell times at different nucleotide concentrations and external force. Predictions are also made for as yet unmeasured quantities, such as the internal strain in the molecule and the randomness ratio. The model also clearly shows how the internal strain can be used by myosin-V to coordinate its forward motion. A clear advantage of our model is that the physical significance of parameters in the model is transparent. This transparency makes the model a useful reference for comparison to future experiments and aids in the identification of elements of the model which are accurate and elements that need refinement. As our work and other recent quantitative studies have demonstrated, it is possible to give a clear analysis of very detailed models. Even when experimental data are

individually not conclusive, the large number of existing experimental measurements available should help to differentiate the models when they are analysed in such detail. In turn this will be useful in clarifying the underlying mechanism of the myosin-V walk, which is still not precisely understood.

We remark that ours is the first attempt to explore carefully whether a full reaction cycle, with a nearly complete list of relevant parameters, is or is not able to reproduce the trends observed over a variety of experimental studies. There are several useful outcomes from our study. With the exception of the dependence of run length on ADP concentration our model does appear to be broadly consistent with the experimental observations. We are still unable to explain even the qualitative nature of the run length dependence on ADP concentration. This is a puzzle, which might signify a flaw in the accepted models and which we flag for future experimental attention. In addition, we find that phosphate release must be coupled to a release of energy over much of the transition between states 3 and 4 if the model is to produce results that are consistent with known rates of Pi release.

Acknowledgments

The authors would like to acknowledge the enormous assistance afforded by one particularly scrupulous and knowledgeable referee. We have also benefitted from discussions with Prof Kolomeisky (Rice), Prof Sun (Hopkins) and Prof Molloy (Mill Hill, London) who was also inspirational in motivating this work. We acknowledge the support of EPSRC through grant GR/S24671/01.

A Analytical Expressions

These expressions were used to compare with experimental data.

The master equations for the probabilities, P_j , of finding the molecule in state j , can be deduced from Fig. 2 to be

$$\dot{P}_1 = u_5 P_5 + w_2 P_2 - (u_1 + w_1) P_1, \quad (24)$$

$$\dot{P}_2 = u_1 P_1 + w_3 P_3 - (u_2 + w_2 + u_{2,7} + w_{2,6}) P_2 + u_{6,2} P_6 + w_{7,2} P_7, \quad (25)$$

$$\dot{P}_3 = u_2 P_2 + w_4 P_4 - (u_3 + w_3) P_3, \quad (26)$$

$$\dot{P}_4 = u_3 P_3 + w_5 P_5 - (u_4 + w_4 + u_{4,6}) P_4 + w_{6,4} P_6, \quad (27)$$

$$\dot{P}_5 = u_4 P_4 + w_1 P_1 - (u_5 + w_5) P_5, \quad (28)$$

$$\dot{P}_6 = u_{4,6} P_4 + w_{2,6} P_2 - (u_{6,2} + w_{6,4}) P_6, \quad (29)$$

$$\dot{P}_7 = u_{2,7} P_2 - (w_{7,2} + u_7) P_7. \quad (30)$$

In matrix notation we have

$$\dot{\mathbf{P}} = \mathbb{M} \mathbf{P}, \quad (31)$$

where \mathbb{M} is the 7x7 reaction rate matrix and the j th component of the vector \mathbf{P} is P_j .

The probability of finding the molecule in one of states 1 to 7 is not conserved under equation (31) since the motor drops off the actin track at a rate u_7 from state 7 (equation (30)). In order to solve equation (31) it is helpful to renormalise, eliminating drop-off, to get a probability-conserving equation. This is done by writing

$$P_j = \frac{1}{\varphi_j} e^{-\lambda t} \tilde{P}_j \quad (32)$$

and choosing the constants φ_j such that the renormalised probabilities \tilde{P}_j satisfy a conservative set of equations. It is possible to show that this can be done (see Ref. (50)) if

$$\mathbb{M}^T \boldsymbol{\varphi} = -\lambda \boldsymbol{\varphi}, \quad (33)$$

and that then the vector $\tilde{\mathbf{P}}$ of renormalised probabilities satisfies the equation

$$\dot{\tilde{\mathbf{P}}} = \tilde{\mathbb{M}} \tilde{\mathbf{P}}, \quad (34)$$

where $\tilde{\mathbb{M}}$ is a renormalised reaction-rate matrix with $\tilde{u}_7 = 0$ and renormalised rate constants

$$\tilde{u}_j = u_j \frac{\varphi_{j+1}}{\varphi_j} \quad \text{and} \quad \tilde{w}_j = w_j \frac{\varphi_{j-1}}{\varphi_j}, \quad (35)$$

for $j = 1 \dots 5$, where the index is periodic with period 5, and

$$\tilde{u}_{i,j} = u_{i,j} \frac{\varphi_j}{\varphi_i} \quad \text{and} \quad \tilde{w}_{i,j} = w_{i,j} \frac{\varphi_j}{\varphi_i}, \quad (36)$$

for the rate constants not on the main reaction cycle.

The slowest, dominant eigenvalue, $-\lambda_0$, is negative for reasonable rate constants, while the faster eigenvalues can be complex giving rise to fast oscillations in the reaction network.

At long times, $\tilde{\mathbf{P}}$ tends to the steady-state solution of equation (34) (50), found by solving $\tilde{\mathbb{M}} \tilde{\mathbf{P}} = 0$ analytically. The relaxation times of oscillations are found to be fast compared to the stepping time and to $1/\lambda_0$, so it is clear from equation (32) that the solution for P_j at long times will be dominated

by the slowest eigenvalue, $-\lambda_0$. We therefore choose φ to be the corresponding eigenvector of the transposed matrix \mathbb{M}^T . Since there are seven states in our model, this eigenvalue problem is best solved numerically.

In the following equations we assume all the rate constants are renormalised and drop the tilde. We look for steady-state solutions $\dot{P}_j = 0$. (For another approach to achieve analytical expressions for a fairly similar reaction network, see Kolomeisky (51)). The net flux between two neighbouring states is given by $J = P_j u_j - P_{j+1} w_{j+1}$, and we seek to express the steady-state probabilities P_j in terms of the futile flux $J_{\text{fut}} = P_6 u_{6,2} - P_2 w_{2,6}$ and the main reaction flux $J_{\text{hyd}} = V/d = P_1 u_1 - P_2 w_2$. It can be shown that the steady-state solution is given by

$$P_j = \frac{\Gamma}{\Gamma - 1} \left[r_j \frac{V}{d} + s_j J_{\text{fut}} \right], \quad (37)$$

for $j = 1, \dots, 5$, $P_7 = (u_{2,7}/w_{7,2})P_2$, and

$$P_6 = \frac{\Gamma_2}{\Gamma_2 - 1} \left[r'_1 J_{\text{fut}} + s'_1 \frac{V}{d} \right], \quad (38)$$

where Γ is given by Eq. (16) and

$$\Gamma_2 = \prod_{j=1}^4 \frac{u'_j}{w'_j} = \frac{u_{6,2} u_2 u_3 u_{4,6}}{w_{6,4} w_{2,6} w_3 w_4} = e^{\Delta G_{\text{hyd}}/k_{\text{B}}T}. \quad (39)$$

Here we have introduced the auxiliary functions

$$r_j = \frac{1}{u_j} \left(1 + \sum_{k=1}^4 \prod_{i=1}^k \frac{w_{j+i}}{u_{j+i}} \right), \quad (40)$$

$$s_j = \frac{1}{u_j} \left((\delta_{j,2} + \delta_{j,3}) + \sum_{k=1}^4 (\delta_{j+k,2} + \delta_{j+k,3}) \prod_{i=1}^k \frac{w_{j+i}}{u_{j+i}} \right), \quad (41)$$

for $j = 1, \dots, 5$, where $\delta_{j,i}$ is the Kronecker delta function (with $\delta_{j,i} \equiv \delta_{j+5,i}$) and where the indices on the rate constants are periodic with period 5. We have similar auxiliary functions relating to the futile cycle, namely

$$r'_j = \frac{1}{u'_j} \left(1 + \sum_{k=1}^3 \prod_{i=1}^k \frac{w'_{j+i}}{u'_{j+i}} \right), \quad (42)$$

$$s'_j = \frac{1}{u'_j} \left((\delta_{j,2} + \delta_{j,3}) + \sum_{k=1}^3 (\delta_{j+k,2} + \delta_{j+k,3}) \prod_{i=1}^k \frac{w'_{j+i}}{u'_{j+i}} \right), \quad (43)$$

for $j = 1, \dots, 4$, where $w'_j = w_j$ and $u'_j = u_j$ except for $w'_1 = w_{6,4}$, $w'_2 = w_{2,6}$, $u'_1 = u_{6,2}$, and $u'_4 = u_{4,6}$. We now have a period of four, $u'_j \equiv u'_{j+4}$, $w'_j \equiv w'_{j+4}$, and $\delta_{j,i} \equiv \delta_{j+4,i}$, since there are four states that participate in the futile cycle (Fig. 1).

Using the conservation of probability $\sum P_j = 1$ (since drop-off has been eliminated through renormalisation) and a second independent expression for P_4 ,

$$P_4 = \frac{\Gamma_2}{\Gamma_2 - 1} \left[r'_4 J_{\text{fut}} + s'_4 \frac{V}{d} \right], \quad (44)$$

one can derive the analytical expressions for the velocity, V , and the futile flux, J_{fut} :

$$V = B d \left(\frac{r'_4}{\Gamma(\Gamma_2 - 1)} - \frac{s_4}{\Gamma_2(\Gamma - 1)} \right), \quad (45)$$

$$J_{\text{fut}} = B \left(\frac{r_4}{\Gamma_2(\Gamma - 1)} - \frac{s'_4}{\Gamma(\Gamma_2 - 1)} \right), \quad (46)$$

where

$$\begin{aligned} \frac{1}{B} = \Gamma \Gamma_2 \left[\left(\frac{\sum_{j=1}^5 \tilde{r}_j}{\Gamma_2(\Gamma - 1)} + \frac{s'_1}{\Gamma(\Gamma_2 - 1)} \right) \left(\frac{r'_4}{\Gamma(\Gamma_2 - 1)} - \frac{s_4}{\Gamma_2(\Gamma - 1)} \right) \right. \\ \left. + \left(\frac{\sum_{j=1}^5 \tilde{s}_j}{\Gamma_2(\Gamma - 1)} + \frac{r'_1}{\Gamma(\Gamma_2 - 1)} \right) \left(\frac{r_4}{\Gamma_2(\Gamma - 1)} - \frac{s'_4}{\Gamma(\Gamma_2 - 1)} \right) \right], \end{aligned} \quad (47)$$

with $\tilde{r}_j = r_j$ and $\tilde{s}_j = s_j$ for $j = 1, 3, 4, 5$, while $\tilde{r}_2 = r_2(1 + u_{2,7}/w_{7,2})$ and $\tilde{s}_2 = s_2(1 + u_{2,7}/w_{7,2})$.

With the probability of finding the molecule in each state now determined, we can use previously established analytical expressions. The fraction of backward steps is (27, 52)

$$\pi_- = \frac{\hat{w}_0 w_1}{\hat{u}_0 u_1 + \hat{w}_0 w_1}, \quad (48)$$

where $\hat{u}_0 = u_5 (P_5 / \sum_{j=2}^7 P_j)$ and $\hat{w}_0 = w_2 (P_2 / \sum_{j=2}^7 P_j)$.

The mean forward-step dwell time is given by (27, 52)

$$t_d = \frac{\hat{u}_0 + u_1 + \hat{w}_0 + w_1}{\hat{u}_0 u_1 + \hat{w}_0 w_1}, \quad (49)$$

and the dispersion is given by (32, 53)

$$D = \frac{1}{2} \left[\frac{\hat{u}_0 u_1}{\hat{w}_0 w_1} + 1 - 2 \left(\frac{\hat{u}_0 u_1}{\hat{w}_0 w_1} - 1 \right) \frac{\hat{w}_0 w_1}{(\hat{u}_0 + u_1 + \hat{w}_0 + w_1)^2} \right] \frac{\hat{w}_0 w_1}{(\hat{u}_0 + u_1 + \hat{w}_0 + w_1)} d^2. \quad (50)$$

Since the probability of the myosin remaining attached to the actin filament decays exponentially with the dominant eigenvalue $-\lambda_0$, the typical duration of a run is $1/\lambda_0$ and hence the run length L is given by

$$L = \frac{V}{\lambda_0}. \quad (51)$$

B Cost Function

The cost function contains 17 terms. Except where other concentrations are explicitly mentioned, the nucleotide concentrations are given by $[\text{ATP}] = 1$ mM and $[\text{ADP}] = [\text{P}_i] = 0.1$ μM . Likewise, the external force is assumed to be zero, except if stated otherwise.

The first term in the cost function is constructed from the model velocity, V , compared to the velocity V^E estimated from experimental data in the literature (11, 12, 14, 15, 23, 25). The mean squared uncertainty in the measured velocities, $\sigma_{V^E}^2$, are in general found to be around 10%.

$$\Delta^{(1)} = \frac{[V - V^E]^2}{\sigma_{V^E}^2} = \frac{[V - 540 \text{ nm/s}]^2}{(54 \text{ nm/s})^2}. \quad (52)$$

When the ADP concentration increases the velocity V^E is found to decrease (12, 14, 15, 19, 23). We choose a second and third ADP concentration, $[\text{ADP}]^{(2)} = 200$ μM and $[\text{ADP}]^{(3)} = 2.5$ mM, and construct additional terms in the cost function at these conditions:

$$\Delta^{(2)} = \frac{[V([\text{ADP}]^{(2)}) - V^E([\text{ADP}]^{(2)})]^2}{\sigma_{V^E([\text{ADP}]^{(2)})}^2} = \frac{[V([\text{ADP}]^{(2)}) - 320 \text{ nm/s}]^2}{(32 \text{ nm/s})^2}. \quad (53)$$

$$\Delta^{(3)} = \frac{[V([\text{ADP}]^{(3)}) - V^E([\text{ADP}]^{(3)})]^2}{\sigma_{V^E([\text{ADP}]^{(3)})}^2} = \frac{[V([\text{ADP}]^{(3)}) - 130 \text{ nm/s}]^2}{(13 \text{ nm/s})^2}. \quad (54)$$

When the ATP concentration decreases the velocity V^E is found to decrease (8, 23). Choosing $[\text{ATP}]^{(2)} = 10$ μM we construct a fourth term:

$$\Delta^{(4)} = \frac{[V([\text{ATP}]^{(2)}) - V^E([\text{ATP}]^{(2)})]^2}{\sigma_{V^E([\text{ATP}]^{(2)})}^2} = \frac{[V([\text{ATP}]^{(2)}) - 75 \text{ nm/s}]^2}{(10 \text{ nm/s})^2}. \quad (55)$$

It is found that changing $[P_i]$ several millimolar does not significantly change the velocity of myosin-V (13, 23). Choosing $[P_i]^{(2)} = 40$ mM, we add a fifth term using measurements by Baker et al. (23):

$$\Delta^{(5)} = \frac{[V([P_i]^{(2)}) - V^E([P_i]^{(2)})]^2}{\sigma_{V^E([P_i]^{(2)})}^2} = \frac{[V([P_i]^{(2)}) - 440 \text{ nm/s}]^2}{(44 \text{ nm/s})^2}. \quad (56)$$

Baker et al. (23) have performed a large number of experiments of the run length L at different nucleotide concentrations finding that the run length is increased with a decrease in the concentration of either ADP or ATP. We introduce four terms to the cost function based on run lengths at different nucleotide concentrations (where $[ATP]^{(3)} = 100 \mu\text{M}$):

$$\Delta^{(6)} = \frac{[L - L^E]^2}{\sigma_{L^E}^2} = \frac{[L - 800 \text{ nm}]^2}{(150 \text{ nm})^2}. \quad (57)$$

$$\Delta^{(7)} = \frac{[L([ADP]^{(3)}) - L^E([ADP]^{(3)})]^2}{\sigma_{L^E([ADP]^{(3)})}^2} = \frac{[L([ADP]^{(3)}) - 400 \text{ nm}]^2}{(150 \text{ nm})^2}. \quad (58)$$

$$\Delta^{(8)} = \frac{[L([ATP]^{(3)}) - L^E([ATP]^{(3)})]^2}{\sigma_{L^E([ATP]^{(3)})}^2} = \frac{[L([ATP]^{(3)}) - 1150 \text{ nm}]^2}{(150 \text{ nm})^2}. \quad (59)$$

$$\Delta^{(9)} = \frac{[L([P_i]^{(2)}) - L^E([P_i]^{(2)})]^2}{\sigma_{L^E([P_i]^{(2)})}^2} = \frac{[L([P_i]^{(2)}) - 500 \text{ nm}]^2}{(150 \text{ nm})^2}. \quad (60)$$

The velocity is found to be independent of external force up to $f_{\text{ex}}^{(2)} = 0.75$ pN (12, 13, 25) and we include an tenth term based on this:

$$\Delta^{(10)} = \frac{[V(f_{\text{ex}}^{(2)}, [ADP]^{(2)}) - V^E(f_{\text{ex}}^{(2)}, [ADP]^{(2)})]^2}{\sigma_{V^E(f_{\text{ex}}^{(2)})}^2} = \frac{[V(f_{\text{ex}}^{(2)}) - V([ADP]^{(2)})]^2}{(50 \text{ nm/s})^2}, \quad (61)$$

where $V([ADP]^{(2)})$ is the velocity in Eq. (53). Similarly, it was found that run length is fairly independent of external force (26), giving the eleventh term:

$$\Delta^{(11)} = \frac{[L(f_{\text{ex}}^{(2)}, [ADP]^{(2)}) - L^E(f_{\text{ex}}^{(2)}, [ADP]^{(2)})]^2}{\sigma_{L^E(f_{\text{ex}}^{(2)})}^2} = \frac{[L(f_{\text{ex}}^{(2)}) - L([ADP]^{(2)})]^2}{(150 \text{ nm})^2}, \quad (62)$$

where $L([\text{ADP}]^{(2)}) = 400 \text{ nm}$ (23). Also dwell time is found to be independent of external force up to $f_{\text{ex}}^{(3)} = 1 \text{ pN}$ (11, 25) giving rise to the twelfth term:

$$\Delta^{(12)} = \frac{[t_{\text{d}}(f_{\text{ex}}^{(3)}, [\text{ADP}]^{(2)}) - t_{\text{d}}^E([\text{ADP}]^{(2)})]^2}{\sigma_{t_{\text{d}}^E(f_{\text{ex}}^{(3)})}^2} = \frac{[t_{\text{d}}(f_{\text{ex}}^{(3)}) - 0.15 \text{ s}]^2}{(0.1 \text{ s})^2}. \quad (63)$$

Rosenfeld and Sweeney (24) found that the release of ADP from the front head is at least 50 times slower than from the rear head, which gives rise to the thirteenth term:

$$\Delta^{(13)} = \frac{1}{50^2} \left(\frac{J_{\text{fut}} d}{V} \right)^2. \quad (64)$$

where J_{fut} is the futile flux (Eq. (46)). The last four terms are restrictions on the possible values of the energy jumps ΔG_i , reflecting some inherent limits caused by strict limits on the energy available in each sub-step of the chemical reaction. Using measurements on S1 (see table 2) as rough ‘target’ values, but allowing for a deviation from these values of $\sigma_{\Delta G_i} = 3 k_{\text{B}} T$ the last four terms are:

$$\Delta^{(14-17)} = \frac{[\Delta G_i - \Delta G_i^{\text{S1}}]^2}{\sigma_{\Delta G_i}^2}. \quad (65)$$

The total cost function is simply defined to be the sum of all the different cost terms:

$$\Delta = \sum_{i=1}^{17} \Delta^{(i)}. \quad (66)$$

All the terms in the cost function cannot be expected to constrain completely independent properties of the model. However, with 17 differing constraints on only nine free parameters it is encouraging, and perhaps not surprising, that the optimization reveals that the best solutions are grouped in the same region of parameter space.

References

1. Sellers, J. R. 1999. Myosins. 2nd edition. Oxford University Press, Oxford.
2. Howard, J. 2001. Mechanics of Motor Proteins and the Cytoskeleton. Sinauer Associates, Sunderland.

3. Bray, D. 2001. *Cell Movements: from molecules to motility*. 2nd edition. Garland, New York.
4. Berg, J. S., B. C. Powell, and R. E. Cheney. 2001. A millennial myosin census. *Mol. Biol. Cell* 12:780–794.
5. Lynn, R. W., and E. W. Taylor. 1971. Mechanism of adenosine triphosphate hydrolysis by actomyosin. *Biochemistry* 10:4617–4624.
6. Cheney, R. E., M. K. O’Shea, J. E. Heuser, M. V. Coelho, J. S. Wolenski, E. M. Espreafico, P. Forscher, R. E. Larson, and M. S. Mooseker. 1993. Brain myosin-V is a two-headed unconventional myosin with motor activity. *Cell* 75:13–23.
7. Forkey, J. N., M. E. Quinlan, M. A. Shaw, J. E. T. Corrie, and Y. E. Goldman. 2003. Three-dimensional structural dynamics of myosin V by single-molecule fluorescence polarization. *Nature* 422:399–404.
8. Yildiz, A., J. N. Forkey, S. A. McKinney, T. Ha, Y. E. Goldman, and P. R. Selvin. 2003. Myosin V walks hand-over-hand: Single fluorophore imaging with 1.5-nm localization. *Science* 300:2061–2065.
9. Snyder, G. E., T. Sakamoto, J. A. Hammer, III, J. R. Sellers, and P. R. Selvin. 2004. Nanometer localization of single green fluorescent proteins: Evidence that myosin V walks hand-over-hand via telemark configuration. *Biophys. J.* 87:1776–1783.
10. Warsaw, D. M., G. G. Kennedy, S. S. Work, E. B. Kremtsova, S. Beck, and K. M. Trybus. 2005. Differential labeling of myosin V heads with quantum dots allows direct visualization of hand-over-hand processivity. *Biophys. J.* 88:L30–L32.
11. Mehta, A. D., R. S. Rock, M. Rief, J. A. Spudich, M. S. Mooseker, and R. E. Cheney. 1999. Myosin-V is a processive actin-based motor. *Nature* 400:590–593.
12. Rief, M., R. S. Rock, A. D. Mehta, M. S. Mooseker, R. E. Cheney, and J. A. Spudich. 2000. Myosin-V stepping kinetics: A molecular model for processivity. *Proc. Natl. Acad. Sci.* 97:9482–9486.
13. Mehta, A. D. 2001. Myosin learns to walk. *J. Cell Science* 114:1981–1998.

14. De La Cruz, E. M., A. L. Wells, S. S. Rosenfeld, E. M. Ostap, and H. L. Sweeney. 1999. The kinetic mechanism of myosin V. *Proc. Natl. Acad. Sci.* 96:13726–13731.
15. De La Cruz, E. M., H. L. Sweeney, and E. M. Ostap. 2000. ADP inhibition of myosin V ATPase activity. *Biophys. J.* 79:1524–1529.
16. De La Cruz, E. M., L. Wells, H. L. Sweeney, and E. M. Ostap. 2000. Actin and light chain isoform dependence of myosin V kinetics. *Biochem.* 39:14196–14202.
17. Trybus, K. M., E. Kremtsova, and Y. Freyzon. 1999. Kinetic characterization of a monomeric unconventional myosin V construct. *J. Biol. Chem.* 274:27448–27456.
18. Sakamoto, T., I. Amitani, E. Yokota, and T. Ando. 2000. Direct observation of processive movement by individual myosin V molecules. *Biochem. Biophys. Res. Commun.* 272:586–590.
19. Wang, F., L. Chen, O. Arcucci, E. V. Harvey, B. Bowers, Y. Xu, J. A. Hammer, III, and J. R. Sellers. 2000. Effect of ADP and ionic strength on the kinetic and motile properties of recombinant mouse myosin V. *J. Biol. Chem.* 275:4329–4335.
20. Walker, M. L., S. A. Burgess, J. R. Sellers, F. Wang, J. A. Hammer, III, J. Trinick, and P. J. Knight. 2000. Two-headed binding of a processive myosin to F-actin. *Nature* 405:804–807.
21. Nishizaka, T., R. Seo, H. Tadakuma, K. Kinosita, and S. Ishiwata. 2000. Characterization of single actomyosin rigor bonds: Load dependence of lifetime and mechanical properties. *Biophys. J.* 79:962–974.
22. Veigel, C., F. Wang, M. L. Bartoo, J. R. Sellers, and J. E. Molloy. 2002. The gated gait of the processive molecular motor, myosin V. *Nature Cell Biol.* 4:59–65.
23. Baker, J. E., E. B. Kremtsova, G. G. Kennedy, A. Armstrong, K. M. Trybus, and D. M. Warshaw. 2004. Myosin V processivity: Multiple kinetic pathways for head-to-head coordination. *Proc. Natl. Acad. Sci.* 101:5542–5546.
24. Rosenfeld, S. S., and H. L. Sweeney. 2004. A model of myosin V processivity. *J. Biol. Chem.* 279:40100–40111.

25. Uemura, S., H. Higuchi, A. Olivares, E. M. De La Cruz, and S. Ishiwata. 2004. Mechanochemical coupling of two substeps in a single myosin V motor. *Nature Struct. Mol. Biol.* 11:877–883.
26. Clemen, A. E.-M., M. Vilfan, J. Jaud, J. Zhang, M. Bärmann, and M. Rief. 2005. Force-dependent stepping kinetics of myosin-V. *Biophys. J.* 88:4402–4410.
27. Kolomeisky, A. B., and M. E. Fisher. 2003. A simple kinetic model describes the processivity of myosin-V. *Biophys. J.* 84:1642–1650.
28. De La Cruz, E. M., and E. M. Ostap. 2004. Relating biochemistry and function in the myosin superfamily. *Curr. Opin. Cell Biol.* 16:61–67.
29. Vale, R. D. 2003. Myosin V motor proteins: marching stepwise towards a mechanism. *J. Cell Biol.* 163:445–450.
30. Vilfan, A. 2005. Elastic lever arm model for myosin V. *Biophys. J.* 88:3792–3805.
31. Lan, G., and S. X. Sun. 2005. Dynamics of myosin-V processivity. *Biophys. J.* 88:999–1007.
32. Fisher, M. E., and A. B. Kolomeisky. 1999. Molecular motors and the forces they exert. *Physica A* 274:241–266.
33. Alberty, R. A., and R. N. Goldberg. 1992. Standard thermodynamic formation properties for the adenosine 5'-triphosphate series. *Biochem.* 31:10610–10615.
34. Jülicher, F., A. Adjari, and J. Prost. 1997. Modeling molecular motors. *Rev. Mod. Phys.* 69:1269–1281.
35. Fisher, M. E. 2005. Kinesin crouches to sprint but resists pushing. *Proc. Natl. Acad. Sci.* 102:16209–16214.
36. Kim, Y. C., and M. E. Fisher. 2005. Vectorial loading of processive motor proteins: implementing a landscape picture. *J. Phys.: Condens. Matter* 17:S3821–S3838.
37. Onsager, L. 1931. Reciprocal relations in irreversible processes. I. *Phys. Rev.* 37:405–426.
38. Geeves, M. A., and K. C. Holmes. 1999. Structural mechanism of muscle contraction. *Annu. Rev. Biochem.* 68:687–728.

39. Houdusse, A., and H. L. Sweeney. 2001. Myosin motors: missing structures and hidden springs. *Curr. Opin. Struc. Bio.* 11:182–194.
40. Nieuwenhuizen, T. M., S. Klumpp, and R. Lipowsky. 2004. Random walks of molecular motors arising from diffusional encounters with immobilized filaments. *Phys. Rev. E* 69:061911–061911.
41. Galassi, M., J. Davies, J. Theiler, B. Gough, G. Jungman, M. Booth, and F. Rossi. 2003. GNU Scientific Library Reference Manual. 2nd edition. Network Theory Ltd, Bristol.
42. Locke, J. C. W., A. J. Millar, and M. S. Turner. 2005. Modelling genetic networks with noisy and varied experimental data: the circadian clock in arabidopsis thaliana. *J. Theor. Biol.* 234:383–393.
43. Landau, L. D., and E. M. Lifshitz. 1986. Theory of elasticity. *In* Course of theoretical physics, volume 7, 3rd edition. Pergamon, Oxford.
44. Howard, J., and J. A. Spudich. 1996. Is the lever arm of myosin a molecular elastic element? *Proc. Natl. Acad. Sci.* 93:4462–4464.
45. Svoboda, K., P. P. Mitra, and S. M. Block. 1994. Fluctuation analysis of motor protein movement and single enzyme kinetics. *Proc. Natl. Acad. Sci.* 91:11782–11786.
46. Barkai, N., and S. Leibler. 1997. Robustness in simple biochemical networks biochemical parameters. *Nature* 387:913–917.
47. Moore, J. R., E. B. Kremontsova, K. M. Trybus, and D. M. Warshaw. 2001. Myosin V exhibits a high duty cycle and large unitary displacement. *J. Cell Biol.* 155:625–635.
48. Geeves, M. A., R. S. Goody, and H. Gutfreund. 1984. Kinetics of acto-S1 interaction as a guide to a model for the crossbridge cycle. *J. Muscle Res. Cell. Motil.* 5:351–361.
49. De La Cruz, E. M., E. M. Ostap, and H. L. Sweeney. 2001. Kinetic mechanism and regulation of myosin VI. *J. Biol. Chem.* 276:32373–32381.
50. Kolomeisky, A. B., and M. E. Fisher. 2000. Periodic sequential kinetic models with jumping, branching and deaths. *Physica A* 279:1–20.
51. Kolomeisky, A. B. 2001. Exact results for parallel-chain kinetic models of biological transport. *J. Chem. Phys.* 115:7253–7259.

52. van Kampen, N. G. 1992. *Stochastic Processes in Physics and Chemistry*. 2nd edition. North-Holland, Amsterdam.
53. Derrida, B. 1983. Velocity and diffusion constant of a periodic one-dimensional hopping model. *J. Stat. Phys.* 31:433–450.

G_2^\ddagger	G_3^\ddagger	G_4^\ddagger	G_5^\ddagger	E_{strain}	αE_{strain}	ΔG_2	ΔG_3	ΔG_4	ΔG_5
0.3	10.4	15.7	5.8	12.8	5.4	0.14	9.9	-10	13.1

Table 1: The estimated values (in units of $k_B T$) of the free parameters in the model as given by the optimisation routine (see also Fig. 4).

ΔG_2^{S1}	ΔG_3^{S1}	ΔG_4^{S1}	ΔG_5^{S1}
2	5.7	-7.7	15.3

Table 2: Energy jumps (in $k_B T$ units) measured for the reaction of S1 with actin (taken from Table 14.2, Ref. (2) using Eq. 2).

Figure Legends

Figure 1.

Sketch of the complete reaction network of the model. The Y-shaped molecule is the myosin-V protein which walks on actin filaments. The black actin monomers indicate the attachment sites spaced at $\simeq 36$ nm. The labels T, D, and P_i stand for ATP, ADP, and inorganic phosphate respectively being bound to the head.

Figure 2.

The main and futile cycles combined in one scheme showing all the reactions paths between the 7 states in the complete model. See also Fig. 1. The reaction rates are given by the corresponding equations in the text. Reaction steps which release and bind ADP, P_i, or ATP are indicated.

Figure 3.

The mechanical movement of myosin-V takes place in two separate steps. The first step, through a distance $d_W \simeq 25$ nm, is from the highly strained state 1 to state 2 where the internal strain balances the external force. When the molecule diffuses to state 3, through a further distance $d_D \simeq 11$ nm, the internal strain increases to bE_{strain} .

Figure 4.

The one dimensional energy landscape that we find for the walk of myosin-V in which the states in the model are indicated by the filled circles. Energy is measured in units of $k_B T$. The energy changes associated with the dashed transitions are E_{strain} and bE_{strain} , being the energy barriers involved in moving away from state 2. Also shown is the rate limiting activation energy G_4^\ddagger between state 4 and state 5. The generalised reaction coordinate X can be thought of as measuring the progress around the main reaction cycle (Fig. 1). As such it reflects a combination of physical motion and the progress of biochemical reactions, according to the substep. The shape of the curve is somewhat arbitrary, but the peaks and the troughs are at the correct energies determined by the optimal values (G_i^\ddagger , E_{strain} , and ΔG_i).

Figure 5.

Predictions of velocity of myosin-V as a function of ADP, ATP, and P_i concentration that arise from our optimised (best) model with parameter values as shown in Table 1 (and used in all subsequent figures). In each case the other two reference concentration are taken from $[ATP] = 1 \text{ mM}$, $[ADP] = 0.1 \text{ } \mu\text{M}$, or $[P_i] = 0.1 \text{ } \mu\text{M}$. The experimental data for varying $[ATP]$ (squares) and $[ADP]$ (circles) are from Baker et al. (23).

Figure 6.

The velocity as a function of force. The solid line (and circles) when $[ATP] = 1 \text{ mM}$ and $[ADP] = 200 \text{ } \mu\text{M}$, the dashed line (and squares) when $[ATP] = 1 \text{ mM}$ and $[ADP] = 1 \text{ } \mu\text{M}$, while for the dotted line (and diamonds) $[ATP] = 10 \text{ } \mu\text{M}$ and $[ADP] = 1 \text{ } \mu\text{M}$. The model (the lines) show similar trends to what is found experimentally (the circles, squares, and diamonds) (25).

Figure 7.

Dwell time for $[ATP] = 2 \text{ mM}$ (solid line/circles), $[ATP] = 10 \text{ } \mu\text{M}$ (dotted line/squares), and $[ATP] = 1 \text{ mM}$ and $[ADP] = 200 \text{ } \mu\text{M}$ (dashed line/triangles). The experimental data are from Mehta et al. (11) (circles) and Uemura et al. (25) (squares and triangles).

Figure 8.

The duty ratio, r_d , as a function of force for $[ATP] = 1 \text{ mM}$, $[ADP] = [P_i] = 0.1 \text{ } \mu\text{M}$.

Figure 9.

Run length L for different concentrations of ATP when the ADP concentration is equal to 1 mM (dotted-dashed line), $100 \text{ } \mu\text{M}$ (dashed line), and $10 \text{ } \mu\text{M}$ (solid line). At low ADP concentration, the run length becomes independent of ATP concentration. The prediction of the model is compared with experimental results at low ADP concentrations (circles) (23).

Figure 10.

Run length L for different strengths of the external force when $[ATP] = 1 \text{ mM}$ and $[ADP] = 200 \text{ } \mu\text{M}$. For negative external force the run length has

a non-monotonic behaviour, where it increases ten fold before decreasing again.

Figure 11.

The fraction of backward steps, $p_{\text{rev}}/p_{\text{for}}$, is insignificant in the model until an external force of ~ 2 pN is reached. The solid line is for $[\text{ATP}] = 2$ mM and $[\text{ADP}] = 200$ μM , while the dashed line is for a reduced ATP concentration of 100 μM .

Figure 12.

The randomness ratio, ρ , as a function of force at different ATP concentrations.

Figure 13.

The circle shows the unperturbed velocity and run length for $[\text{ATP}] = 1$ mM, $[\text{ADP}] = [\text{P}_i] = 0.1$ μM and zero external force. The squares show the influence on run length and velocity of changes of $\pm 5\%$ in each of the nine free parameters of the model (while keeping the other parameters fixed). The run length is very sensitive to changes in G_4^\ddagger . Also perturbing in E_{strain} gives quite large change in run length. Large variation in velocity was only observed when perturbing the parameter ΔG_4 .

Figure 14.

Temperature dependence of velocity and run length (when $[\text{ATP}] = 1$ mM and $[\text{ADP}] = 200$ μM). The model predicts an increase in velocity with temperature, but a decrease of the run length. The velocity is found to be more sensitive to changes in temperature than the run length.

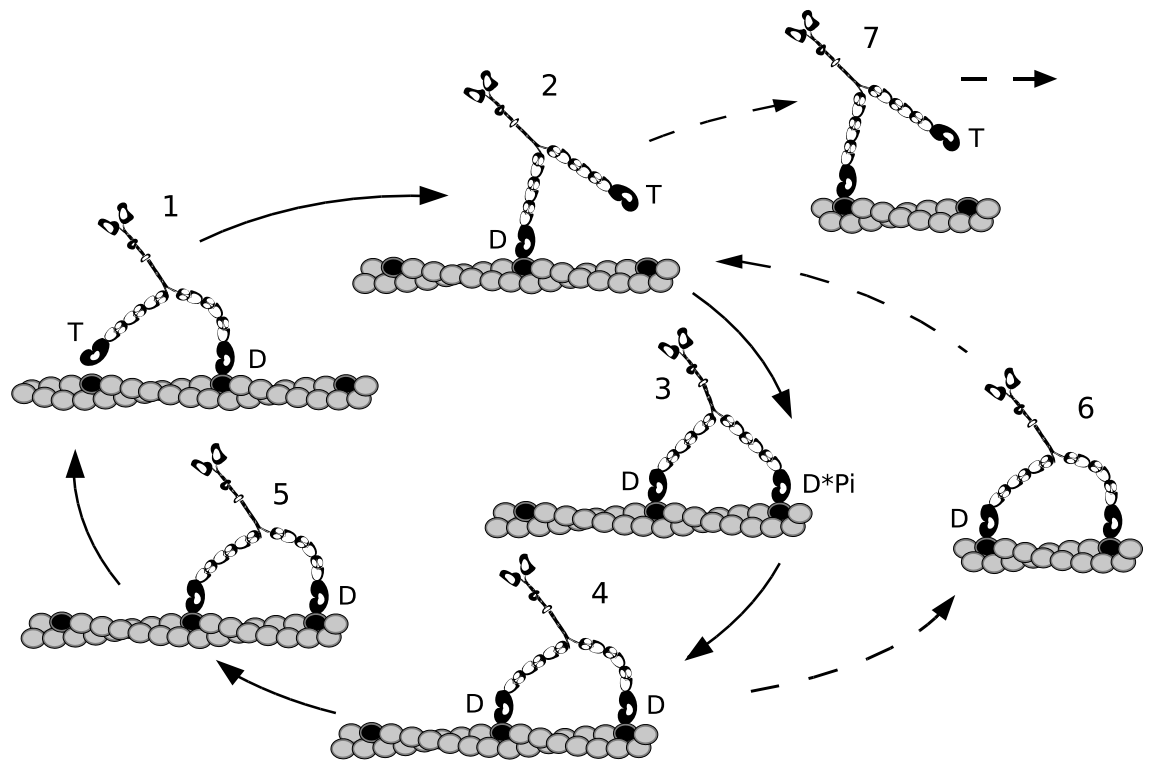


Figure 1:

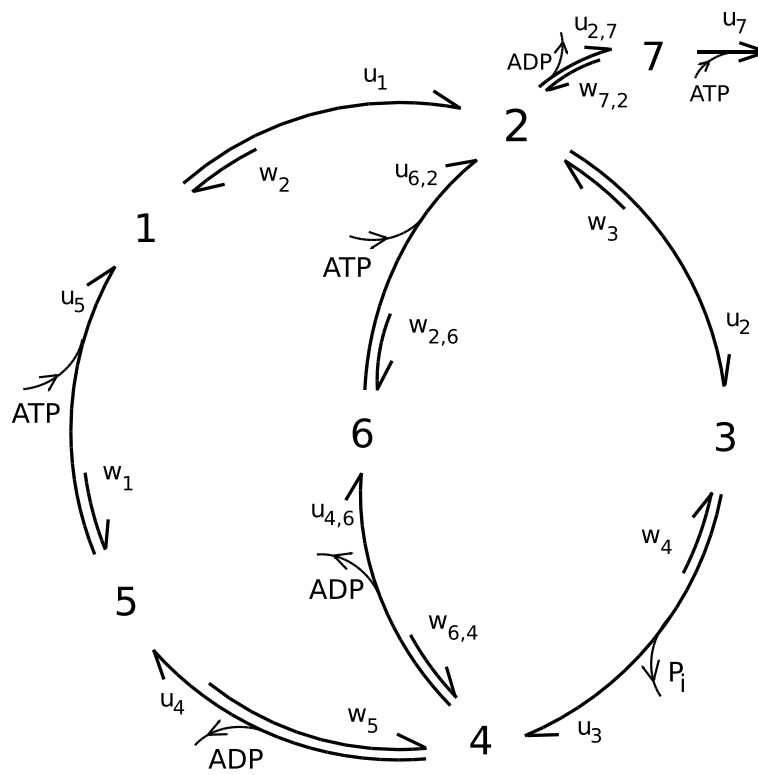


Figure 2:

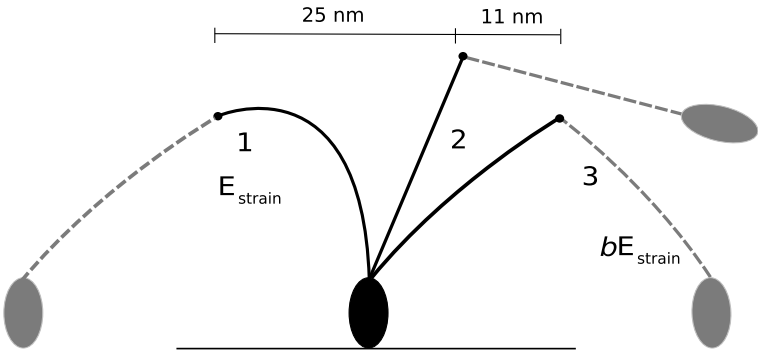


Figure 3:

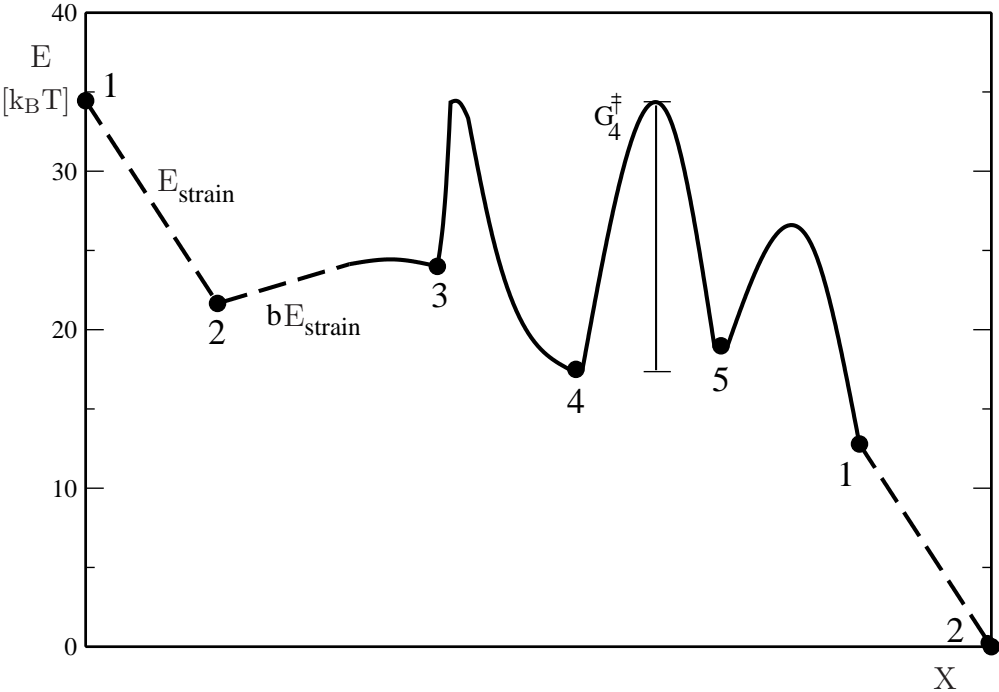


Figure 4:

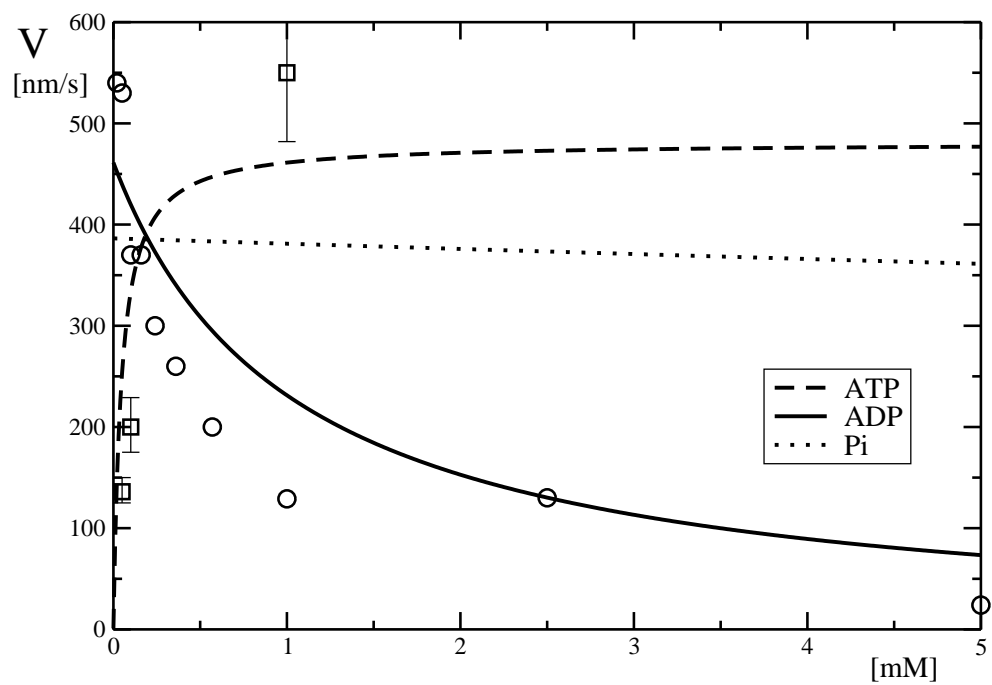


Figure 5:

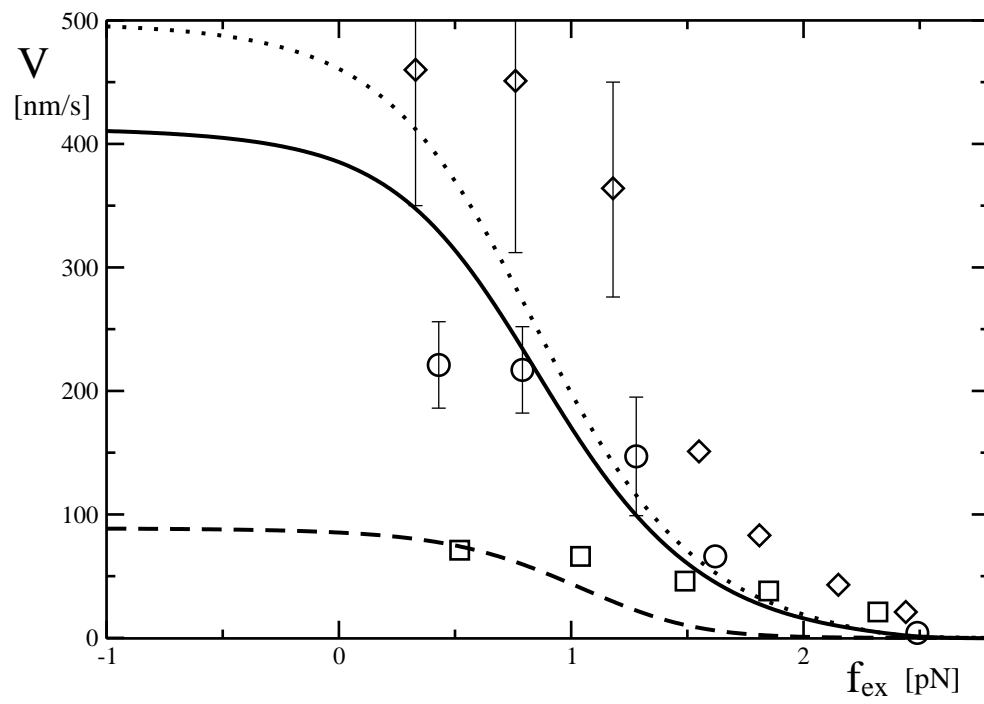


Figure 6:

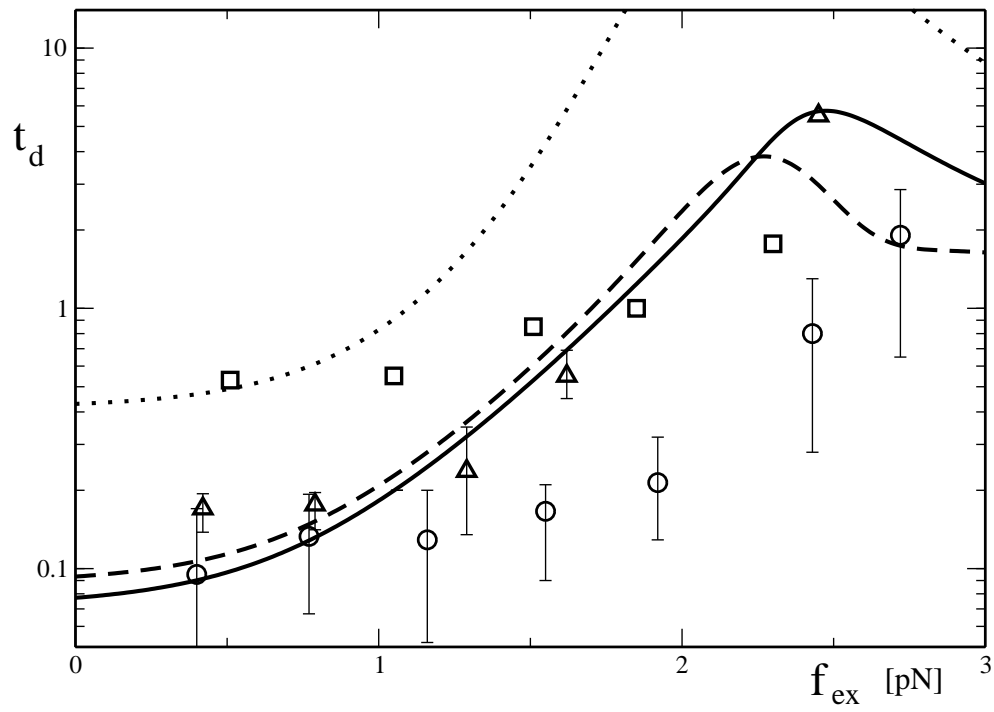


Figure 7:

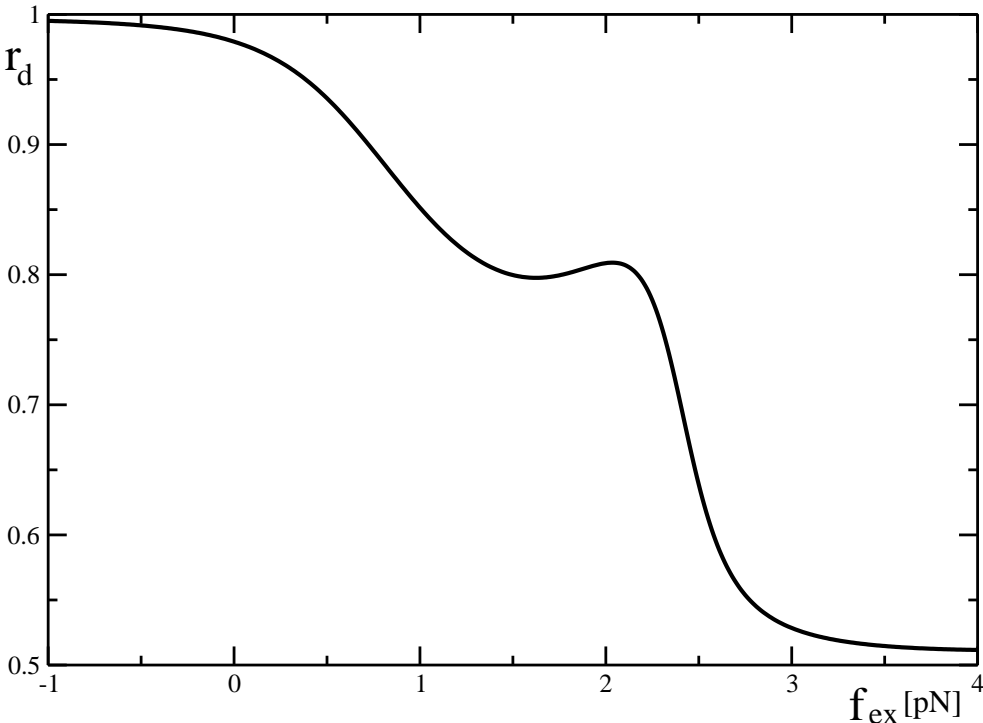


Figure 8:

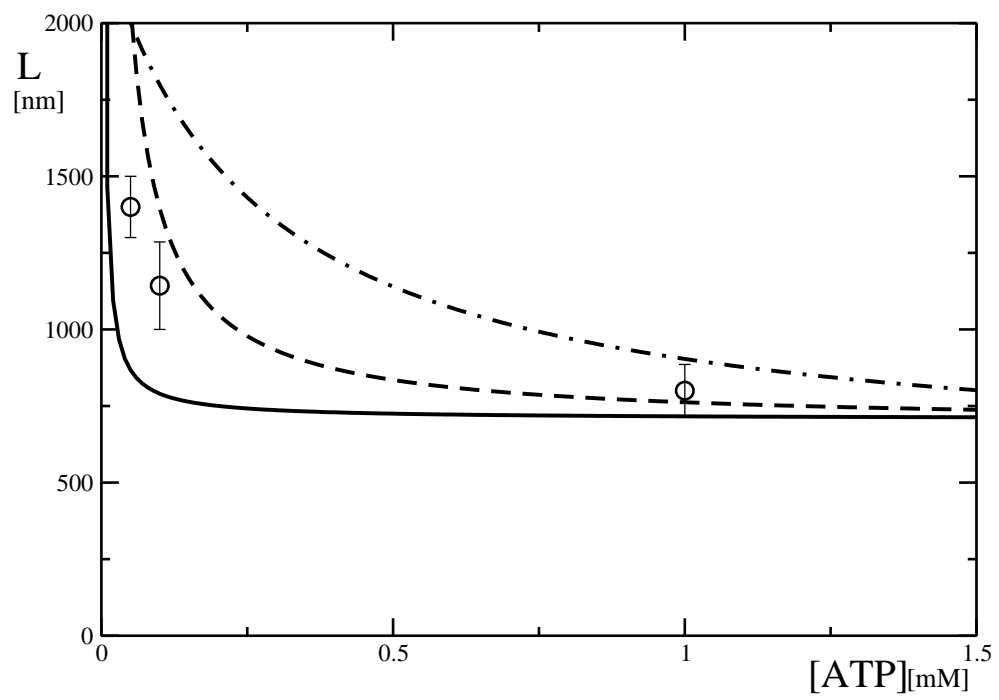


Figure 9:

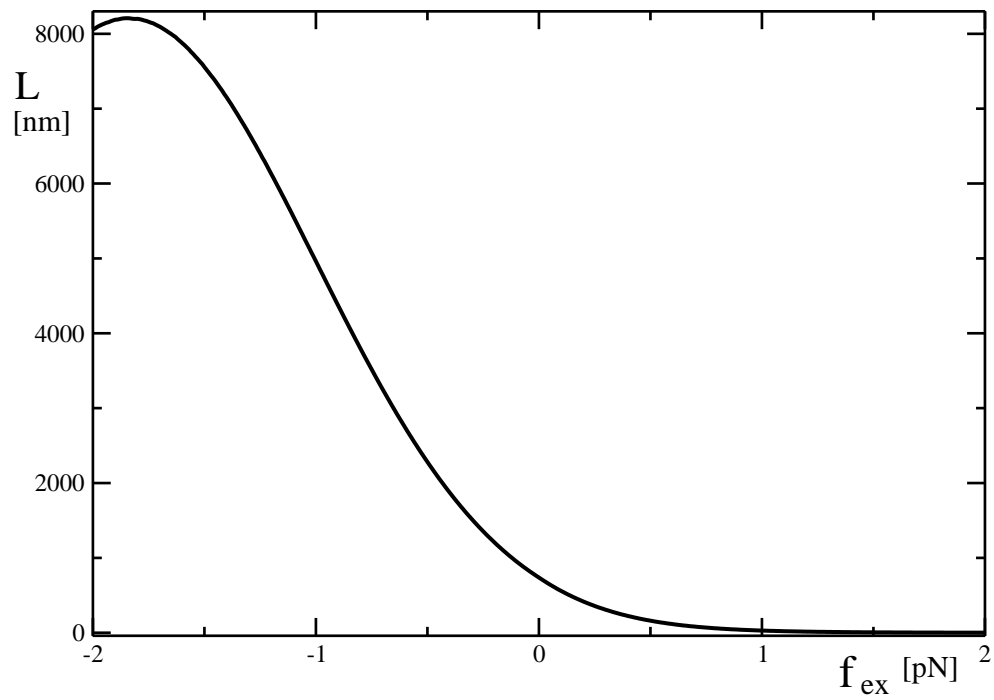


Figure 10:

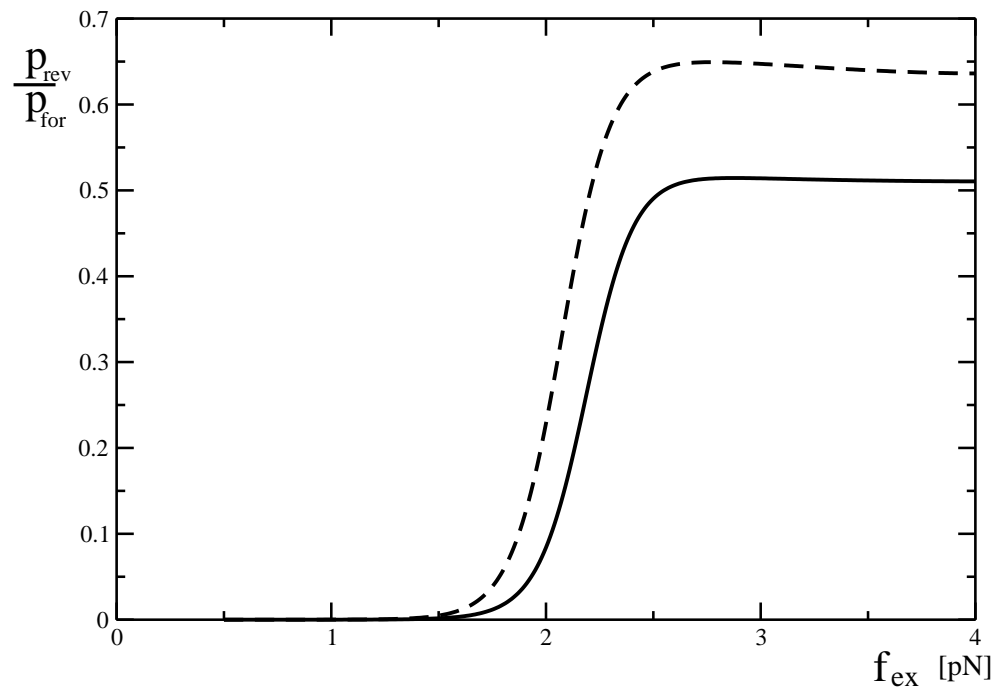


Figure 11:

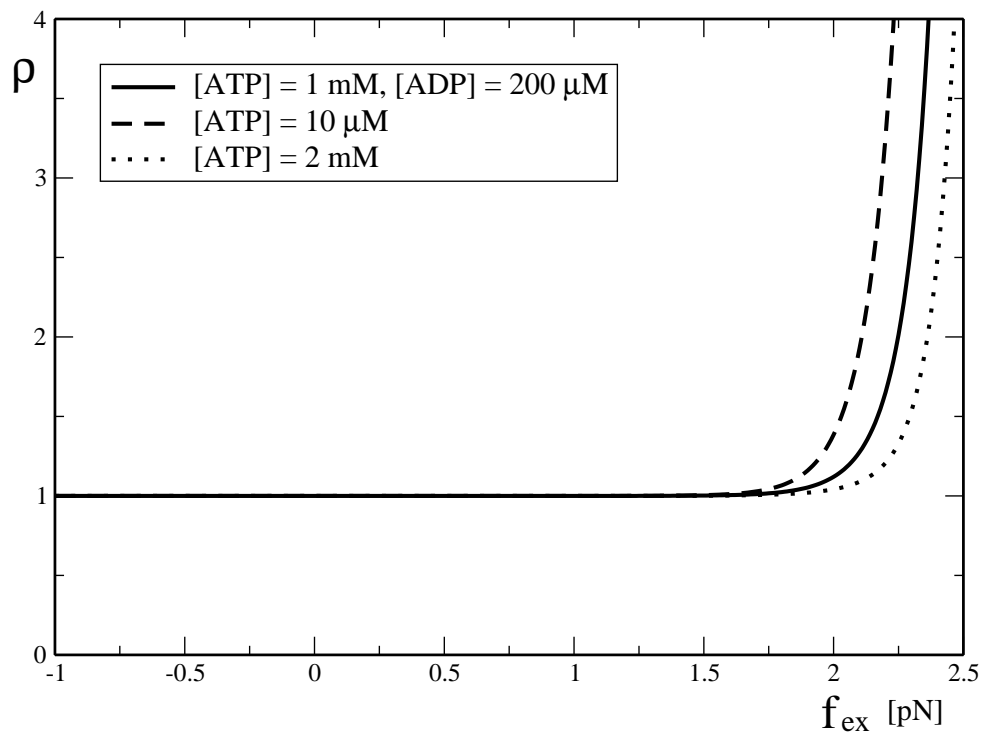


Figure 12:

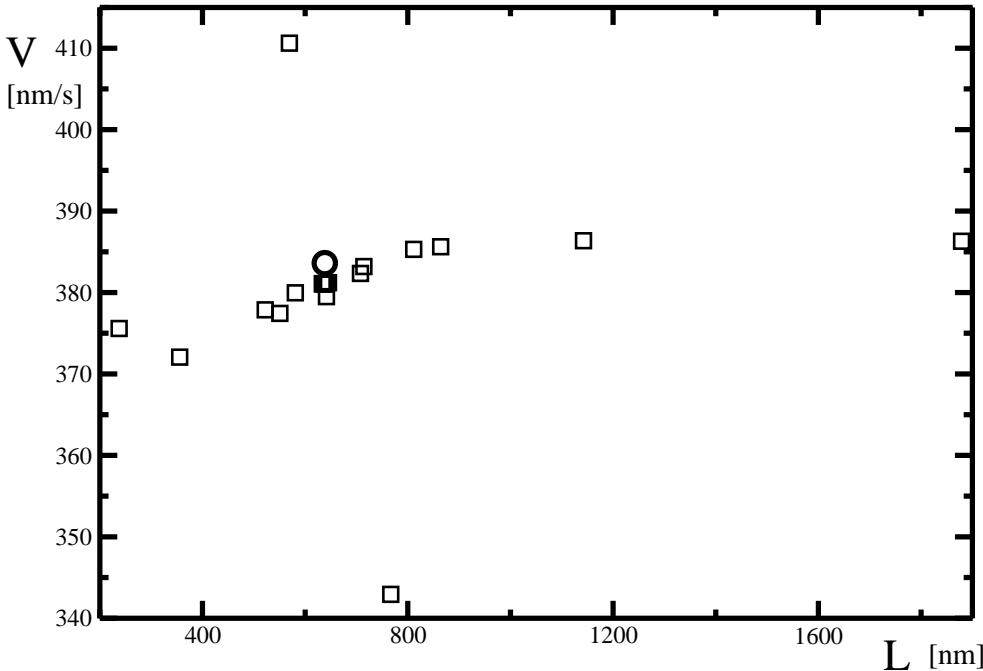


Figure 13:

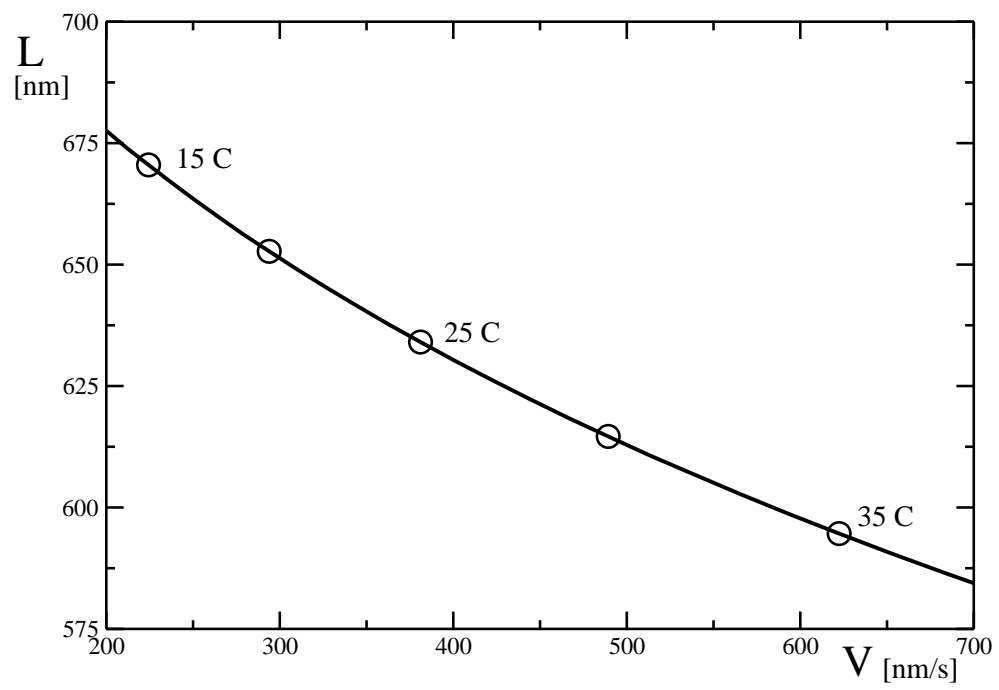


Figure 14: